A DIRECT LYAPUNOV APPROACH TO STABILIZATION AND TRACKING OF UNDERACTUATED MECHANICAL SYSTEMS

by

JASPEN PATENAUDE

B.S., Kansas State University, 2006

A THESIS

submitted in partial fulfillment of the requirements for the degree

MASTER OF SCIENCE

Department of Mechancal Engineering
College of Engineering

KANSAS STATE UNIVERSITY
Manhattan, Kansas

2008

Approved by:

Major Professor
Dr. Warren N. White

Abstract

Mechanical systems play an integral part in our everyday lives. A subset of these systems can be described as underactuated; the defining characteristic of underactuated mechanical systems is that they have fewer control inputs than degrees of freedom. Airplanes, rockets, helicopters, overhead crane loads, surface vessels, and underwater vehicles are all examples of such systems. The control challenges associated with these systems arise from both the underactuation of the control input and the nonlinear nature of the dynamic equations describing the system's motion.

In this work, a control method for stabilization and tracking based on Lyapunov stability theory is presented. The remarkable result of this tracking controller development is that we arrive at three matching equations that are (with the exception of $\overline{\boldsymbol{K}}_D$) identical to matching equations developed for stabilization as shown in White et al. (2006, 2007, 2008). Asymptotic stabilization of the tracking errors ($\boldsymbol{s}$) is not obtained. However, the norm of $\boldsymbol{s}$ ($\|\boldsymbol{s}\|$) will decrease until an ultimate bound is reached, then it will stay within this bound. A lemma is provided for estimating this bound and it is shown that the magnitude of the bound depends upon the eigenvalues and norms of certain matrices in the Lyapunov formulation.

Three examples are presented to illustrate the effectiveness of the direct Lyapunov approach. Two examples of holonomic systems are presented. The first is an inverted pendulum cart which is used to illustrate the formulations performance to tracking a desired path on the cart position or actuated axis. The second example is a ball and beam system in which a desired path is tracked by the ball or unactuated axis.

The tracking control technique is also applied to an example of a nonholonomic system, a rolling wheel. The control technique is applied in two alternate manners. Finally, the controller is implemented on a laboratory inverted pendulum cart system in hard real time. A desired trajectory for the cart position is tracked and the control law is used to define the desired pendulum trajectory.

Table of Contents

List of Figures

List of Tables

Acknowledgements

I would like to personally thank my faculty committee for their support, experience, and wisdom. I would especially like to thank my Major Professor, Dr. Warren White, for giving me the opportunity to work in the area of nonlinear controls. I have found this field to be quiet interesting and very challenging. I would also like to thank him for all of his help and guidance during graduate school.

I am also indebted to Deyka Garcia for her help in reviewing this work. I would like to wish her the best of luck in finishing her PHD studies. To my family, I would like to express my sincere thanks for their continued support of my academic endeavors. While they may not have always understood the difficulties I was facing, they always provided me with support and encouragement for which I will be eternally grateful.

CHAPTER 1 - Introduction

Mechanical systems play an integral part in our everyday lives. A vast quantity of mechanical systems such as automobiles, aircraft, and cranes are employed everyday for transportation or material handling. A subset of these systems can be described as underactuated; this chapter discusses the qualities of such systems, provides examples, and contains a review of work that has been done in recent years to advance control theory in the area of underactuated mechanical systems.

The defining characteristic of underactuated mechanical systems is that they have fewer control inputs than degrees of freedom. Recently there has been extensive research in the control of the underactuated mechanical systems due to the broad range of available applications. Many everyday mechanical systems are underacuated. Airplanes, rockets, helicopters, overhead crane loads, surface vessels, and underwater vehicles are all examples of such systems. The control challenges associated with these systems arise from both the underactuation of the control input and the nonlinear nature of the dynamic equations describing the system's motion. In general, these systems can have holonomic and/or nonholonomic constraints. The equations of motion can be determined from the Euler-Lagrange equation,

$$\frac{d}{dt}\left(\frac{\partial L(\boldsymbol{q},\dot{\boldsymbol{q}})}{\partial \dot{\boldsymbol{q}}}\right)-\frac{\partial L(\boldsymbol{q},\dot{\boldsymbol{q}})}{\partial \boldsymbol{q}}=\boldsymbol{Q}' \tag{1.1}$$

where the vector $\boldsymbol{q}\in\Re^n$ is a vector of generalized coordinates. $L(\boldsymbol{q},\dot{\boldsymbol{q}}):\Re^{2n}\rightarrow\Re$ is the Lagrangian defined as the kinetic energy minus the potential energy of the mechanical system. The vector $\boldsymbol{Q'}$ contains the constraints and applied control input forces/moments (Greenwood, 2003).

For fully actuated systems, a broad range of techniques for optimal, robust, and adaptive control have been developed in the last two decades. These techniques rely on a number of useful system properties inherent in fully actuated systems such as feedback linearizability, passivity, and linear parametrizability. For underactuated systems, these properties may not exist; furthermore, undesirable properties such as higher relative degree (Khalil, 2002) and non-minimum phase behavior may be present. The absence of some of these useful system properties

and the addition of unwanted ones make control design for underactuated systems very challenging.

The research conducted on the control of underactuated mechanical systems usually address either stabilization or tracking. The goal of stabilization is to drive a disturbed system back to a nominal equilibrium point, while tracking addresses the problem of having the system follow a predetermined path or trajectory. Stabilization was once the primary focus of control researchers such as Bloch, Leonard, and Marsden (2000, 2001) with controlled Lagrangians, Olfati-Saber (1998, 2000, and 2001) with backstepping, Ortega, Spong, Gómez-Estern, Blankenstein (2002) in addition to Acosta, Ortega, Astolfi and Mahindrakar (2005) with interconnection damping assignment – passivity based control (IDA-PBC), Auckly, Kapistanki, and White (2000) with the λ method, and White, Foss, Patenaude, Xin, and Garcia (2008) with the direct Lyapunov approach (DLA). However, research in tracking control of underactuated systems is starting to see more activity.

Non-matching Based Approaches

Recent developments of continuous nonlinear tracking control design approaches for underactuated mechanical systems can be categorized into two main areas, matching based and non-matching based. Non-matching based approaches to underactuated system tracking include the work of Driessen and Sadegh (2000) where optimal control techniques were used for minimum time path following of an underactuated manipulator. Their computations were made possible by linearization of the system about the trajectory.

Path following applications for fully actuated systems have also influenced the approaches taken for underactuated systems. A number of researchers have considered inverse dynamics in developing a path for which the trajectory history of each axis is found in advance. Blajer and Kolodziejczyk (2007) developed a feed forward control scheme based on inverse dynamics for their gantry crane applications. It should be noted that the inverse dynamics for underactuated systems are complicated by the reduction in the possible paths caused by the underactuation. These complications have led researchers to try other methods that avoid the need for such calculations.

A notable contribution in the area of non-matching based techniques was made by Sandoz, Kokotović, and Hespanha (2008) with their trackablity filter scheme. This approach

employs a filter which produces an augmented reference signal derived from a nominal input. This new signal is zero error trackable by the underactuated system provided that its zero dynamics are input to state stable (ISS). Alternatively, Ashrafiuon, and Erwin (2004) presented a sliding mode control approach which can drive an underactuated system onto a sliding surface. Lyapunov theory was used to develop the controller used to reach the sliding surface, however asymptotic stability of the sliding surface was not established for the general case. The determination of asymptotically stable surfaces could prove to be a limitation of this technique. In Boskovic and Krstic (1999), a Lyapunov based control law is developed for attitude/position regulation of a six degree of freedom, nonholonomic underwater vehicle. While the controller was designed for fixed point regulation, the tracking error remained small for slowly varying desired trajectories. For faster moving trajectories, this controller could not be expected to perform as well.

Backstepping has also proven to be a popular tool for the design of tracking controllers. Do, Jiang, and Pan (2002) employed this technique in the derivation of a controller for an underactuated surface ship that would asymptotically track a reference trajectory of straight line or curve segments. In Hongrui, Yantao, Siyan, and Zhen (2008) a backstepping technique is applied to a ball and plate system for stabilization and tracking. The authors were successful in tracking a curved reference trajectory with the ball while stabilizing the plate. The backstepping control approach used was dependent upon the system dynamics being expressed in strict-feedback form. While backstepping has proven effective on a case by case basis, it relies heavily upon the designer's creativity in handling undesirable terms from the dynamic equations.

Matching Based Approaches

Research on extending matching equation based stabilization techniques to tracking has also been increasing recently. For example, in Singhal, Patayane, Banavar (2006), the authors derive tracking controllers using the method of interconnection damping assignment-passivity based control (IDA-PBC) and a direct Lyapunov approach and they compared the performance of the two controllers. These controllers were limited in application due to the zero acceleration assumption for the desired trajectory. In Wang and Goldsmith (2008), an IDA-PBC formulation was presented that contained an additional matching equation allowing for tracking control of underactuated port-controlled Hamiltonian (PCH) systems (without the zero acceleration

assumption). However, the authors did make use of inverse dynamics in their development so that the path following techniques of Slotine and Li (1988) could be applied to fully actuated systems.

The goal of this work is to develop a systematic framework for nonlinear controller design that could be applied to holonomic and nonholonomic systems without requiring inverse dynamics. For a system having n degrees of freedom, the controller design method assumes that only m of the degrees of freedom have a specified smooth trajectory history. These histories might be determined by a rudimentary path planner given the initial and ending system configurations or by some similar method. Smoothness of the path is required due to the necessity of determining the velocity and acceleration of each degree of freedom having a specified history. The attractiveness of the approach is that given the m specified histories, the control law to be presented will determine, at each point of time, suitable kinematic values for the $n - m$ degrees of freedom not having specified trajectory histories. This aspect of the control law saves the designer the effort of having to generate these trajectories from inverse dynamics prior to the start of the motion and thus decreasing the response time to handle trajectory changes.

Part of the path following control law presented by Slotine and Li (1988) is the starting point for the controller design. Given the form of the control law, the dynamics of the system are recast in terms of a sliding mode. The control law for the new dynamic equation is developed from a direct Lyapunov approach very similar to that presented in White et al. (2008). Once the control law for the sliding mode dynamic equation is known, it can be incorporated into the original path following control law. Because the path following control law is to be applied to an underactuated system, $n - m$ of the components of the control law vector must be identically zero. These control law equations allow the determination of the accelerations associated with the desired path of the degrees of freedom having unspecified histories. Integration of these accelerations determines the velocities and positions on the unspecified axes. It is demonstrated that there is an upper bound on the norm of the sliding mode variable and thus the error is not asymptotically stable. This bound is partially dictated by the eigenvalues of certain matrices used in the Lyapunov formulation.

In the following chapter, the derivation of the control law and a discussion of the expected performance are presented. In Chapter 3, two examples of holonomic systems are

provided. A DLA controller is derived to drive the system along a desired trajectory. In Chapter 4, a nonholonomic example is presented and the control law is once again derived to drive the system along a desired trajectory. The response of the systems is simulated using Matlab SIMULINK. Chapter 5 contains a hard real time implementation of the DLA control scheme on an inverted pendulum cart. The dynamic model is presented and system identification is performed to determine several unknown parameters. Finally, a desired path is defined for the cart position and the experimental results are presented. In Chapter 6, conclusions and recommendations are presented to improve the DLA controller tracking performance and ease of design.

CHAPTER 2 - Lyapunov Formulation

This chapter details the development of the Lyapunov formulation. Discussion on how certain terms that are introduced to the formulation are dealt with is presented along with the expected system performance when following a path.

The Matching Equations

The mechanical system is described by the nonlinear matrix equation

$$\boldsymbol{M}(\boldsymbol{q})\ddot{\boldsymbol{q}} + \boldsymbol{C}(\boldsymbol{q},\dot{\boldsymbol{q}})\dot{\boldsymbol{q}} + \boldsymbol{C}_{\boldsymbol{D}}\dot{\boldsymbol{q}} + \boldsymbol{G}(\boldsymbol{q}) = \begin{bmatrix} \boldsymbol{\tau} \\ 0 \end{bmatrix} \tag{2.1}$$

where the vector $\boldsymbol{q} \in \Re^n$ is a set of generalized coordinates for the n degrees of freedom of the mechanical system while the time derivative of $\boldsymbol{q}$ specifies the n generalized velocities. The right-hand side of (2.1) contains the vector $\boldsymbol{\tau} \in \Re^m$ where $m<n$ for underactuated systems. It is assumed that the degrees of freedom are ordered so that the first m elements of the right side vector contain the nonzero inputs. Also in (2.1), $\boldsymbol{M}(\boldsymbol{q}) \in \Re^{n\times n}$ is the positive definite mass and/or inertia matrix, $C(\boldsymbol{q},\dot{\boldsymbol{q}})\dot{\boldsymbol{q}} \in \Re^n$ consists of centripetal and Coriolis forces and/or moments, and $\boldsymbol{G}(\boldsymbol{q}) \in \Re^n$ consists of forces and/or moments stemming from gradients of conservative fields.

The requirement of the control law is to both stabilize and drive the system along the specified trajectory. The tracking controller presented by Slotine and Li (1988) was developed for fully actuated systems. In order to apply this sliding mode approach to underactuated systems, modifications of the original controller must be made. The proposed control law for an underactuated system is

$$\begin{bmatrix} \boldsymbol{\tau} \\ 0 \end{bmatrix} = \boldsymbol{M}(\boldsymbol{q})\ddot{\boldsymbol{q}}_r + \boldsymbol{C}(\boldsymbol{q},\dot{\boldsymbol{q}})\dot{\boldsymbol{q}}_r + \boldsymbol{C}_{\boldsymbol{D}}\dot{\boldsymbol{q}}_r - \overline{\boldsymbol{K}}_D\boldsymbol{s} + \begin{bmatrix} \boldsymbol{u}_1 + \boldsymbol{F} \\ \boldsymbol{u}_2 \end{bmatrix} + \boldsymbol{P}(t)^{-1}\nabla\Phi(\boldsymbol{q}) \tag{2.2}$$

Where the matrix $\overline{\boldsymbol{K}}_D \in \Re^{n\times n}$ is a positive definite, Hermitian matrix, $\Phi(\boldsymbol{q})$ is a real scalar potential function of the generalized coordinates, $\boldsymbol{P}(t) \in \Re^{n\times n}$ is a positive definite matrix, and the gradient is computed with respect to the generalized coordinates. The vector $\boldsymbol{u}$, which refers

to the vector $[\boldsymbol{u}_1\ \boldsymbol{u}_2]^{\mathrm{T}}$, is used to provide stabilization to the lower *n-m* equations of (2.2). The vectors $\dot{\boldsymbol{q}}_r$ and $\ddot{\boldsymbol{q}}_r$ are the reference velocity and acceleration, respectively where

$$\dot{\boldsymbol{q}}_r = \dot{\boldsymbol{q}}_d - \boldsymbol{\Lambda}\tilde{\boldsymbol{q}} = \dot{\boldsymbol{q}}_d - \boldsymbol{\Lambda}\left(\boldsymbol{q} - \boldsymbol{q}_d\right). \tag{2.3}$$

In equation (2.3), $\boldsymbol{q}_d$ is the vector of desired coordinate positions and $\boldsymbol{\Lambda} \in \Re^{n\times n}$ is a constant, positive definite, and symmetric matrix. When comparing (2.2) to the control law presented by Slotine and Li (1988), it is seen that the gravitational term is not included in (2.2) and that there are additional terms included which are necessary due to the underactuation. The gravitational term will be seen at a later point to be related to part of $\boldsymbol{F}$ and the gradient of $\Phi(\boldsymbol{q})$. Taking the time derivative of (2.3) produces the reference acceleration. The quantity $\tilde{\boldsymbol{q}}$ consists of the difference between the actual and the desired coordinates and this together with its time derivative constitute the tracking errors. The sliding mode vector $\boldsymbol{s}$ is given by

$$\boldsymbol{s} = \dot{\boldsymbol{q}} - \dot{\boldsymbol{q}}_r = \dot{\tilde{\boldsymbol{q}}} + \boldsymbol{\Lambda}\tilde{\boldsymbol{q}}\,. \tag{2.4}$$

If the control drives the sliding mode vector to the sliding surface where the vector $\boldsymbol{s}$ vanishes, we see that the tracking error then decays to zero.

Combining equations (2.1) and (2.2) yields

$$\begin{aligned}\boldsymbol{M}(\boldsymbol{q})\ddot{\boldsymbol{q}} + \boldsymbol{C}(\boldsymbol{q},\dot{\boldsymbol{q}})\dot{\boldsymbol{q}} + \boldsymbol{C}_D\dot{\boldsymbol{q}} + \boldsymbol{G}(\boldsymbol{q}) &= \boldsymbol{M}(\boldsymbol{q})\ddot{\boldsymbol{q}}_r + \boldsymbol{C}(\boldsymbol{q},\dot{\boldsymbol{q}})\dot{\boldsymbol{q}}_r \\ &+ \boldsymbol{C}_D\dot{\boldsymbol{q}}_r - \overline{\boldsymbol{K}}_D\boldsymbol{s} + \begin{bmatrix}\boldsymbol{u}_1 + \boldsymbol{F} \\ \boldsymbol{u}_2\end{bmatrix} + \boldsymbol{P}(t)^{-1}\nabla\Phi(\boldsymbol{q}).\end{aligned} \tag{2.5}$$

Canceling like terms and using the definitions from (2.3) and (2.4) reduces the last result to

$$\boldsymbol{M}(\boldsymbol{q})\dot{\boldsymbol{s}} + \boldsymbol{C}(\boldsymbol{q},\dot{\boldsymbol{q}})\boldsymbol{s} + \boldsymbol{C}_D\boldsymbol{s} + \boldsymbol{G}(\boldsymbol{q}) = -\overline{\boldsymbol{K}}_D\boldsymbol{s} + \begin{bmatrix}\boldsymbol{u}_1 + \boldsymbol{F} \\ \boldsymbol{u}_2\end{bmatrix} + \boldsymbol{P}(t)^{-1}\nabla\Phi(\boldsymbol{q}). \tag{2.6}$$

The direct Lyapunov approach (White et al. 2006, 2007, 2008) is used to complete the design of the control law for the system. The candidate Lyapunov function is

$$V = \frac{1}{2}\boldsymbol{s}^T\boldsymbol{K}_D\boldsymbol{s} \tag{2.7}$$

where

$$\boldsymbol{K}_D = \boldsymbol{P}(t)\boldsymbol{M}(\boldsymbol{q}), \tag{2.8}$$

and $\boldsymbol{P}(t)$ is a positive definite matrix defined so that $\boldsymbol{K}_D \in \Re^{n\times n}$ is a symmetric, positive matrix. This matrix was seen previously in the control law stated in (2.5). Computing the time derivative of candidate Lyapunov function (2.7) produces

$$\dot{V} = \boldsymbol{s}^T \boldsymbol{K}_D \dot{\boldsymbol{s}} + \frac{1}{2}\boldsymbol{s}^T \dot{\boldsymbol{K}}_D \boldsymbol{s} = -\boldsymbol{s}^T \boldsymbol{K}_v \dot{\boldsymbol{s}} + \Psi(\boldsymbol{s},\boldsymbol{u}) \le 0 \tag{2.9}$$

where $\boldsymbol{K}_v \in \Re^{n\times n}$ is symmetric and at least positive semi-definite, and $\boldsymbol{u}$ again refers to the vector $[\boldsymbol{u}_1\ \boldsymbol{u}_2]^{\mathrm{T}}$ on the right side of (2.6), Ψ and $\boldsymbol{u}$ will be defined later in the analysis. Substituting the time derivative of $\boldsymbol{s}$ from (2.6) into (2.9), we obtain

$$\begin{aligned}\dot{V} &= \boldsymbol{s}^T \boldsymbol{K}_D \boldsymbol{M}^{-1}(\boldsymbol{q})\left(-\boldsymbol{C}(\boldsymbol{q},\dot{\boldsymbol{q}})\boldsymbol{s} - \boldsymbol{C}_D\boldsymbol{s} - \boldsymbol{G}(\boldsymbol{q}) - \overline{\boldsymbol{K}}_D\boldsymbol{s} + \begin{bmatrix}\boldsymbol{u}_1 + \boldsymbol{F}\\ \boldsymbol{u}_2\end{bmatrix} + \boldsymbol{P}(t)^{-1}\nabla\Phi(\boldsymbol{q})\right) + \frac{1}{2}\boldsymbol{s}^T\dot{\boldsymbol{K}}_D\boldsymbol{s} \\ &= -\boldsymbol{s}^T\boldsymbol{K}_v\boldsymbol{s} + \Psi(\boldsymbol{s},\boldsymbol{u}).\end{aligned} \tag{2.10}$$

Following a procedure similar to that of White et al. (2008), we decompose (2.10) into three matching equations. Defining the control input $\boldsymbol{F}$ as

$$\boldsymbol{F} = \boldsymbol{F}_1 + \boldsymbol{F}_2 + \boldsymbol{F}_3 \tag{2.11}$$

where $\boldsymbol{F}_{\mathrm{i}}$ will be used with the i^{th} matching equation. With the substitution of (2.11) into (2.10) we define the first matching equation as

$$\boldsymbol{s}^T\boldsymbol{K}_D\boldsymbol{M}(\boldsymbol{q})^{-1}\left(-\boldsymbol{C}(\boldsymbol{q},\dot{\boldsymbol{q}})\boldsymbol{s} + \begin{bmatrix}\boldsymbol{F}_1\\ 0\end{bmatrix}\right) + \frac{1}{2}\boldsymbol{s}^T\dot{\boldsymbol{K}}_D\boldsymbol{s} = 0, \tag{2.12}$$

the second matching equation as

$$s^T\boldsymbol{K}_D\boldsymbol{M}(\boldsymbol{q})^{-1}\left(\left(-\boldsymbol{C}_D - \overline{\boldsymbol{K}}_D\right)\boldsymbol{s} + \begin{bmatrix}\boldsymbol{F}_2\\ 0\end{bmatrix}\right) = -\boldsymbol{s}^T\boldsymbol{K}_v\boldsymbol{s}, \tag{2.13}$$

and finally the third matching equation as

$$\boldsymbol{s}^T\boldsymbol{K}_D\boldsymbol{M}^{-1}(\boldsymbol{q})\left(-\boldsymbol{G}(\boldsymbol{q}) + \begin{bmatrix}\boldsymbol{F}_3\\ 0\end{bmatrix} + \boldsymbol{P}(t)^{-1}\nabla\Phi(\boldsymbol{q})\right) = 0. \tag{2.14}$$

The First Matching Equation

Two symmetric matrices $\boldsymbol{C}_D^{'} \in \Re^{n\times n}$ and $\overline{\boldsymbol{C}}_D \in \Re^{n\times n}$ are subtracted from the first matching equation and added to the second. These matrices will aid in the solution of these two matching equations. The first two matching equations are rewritten as

$$\boldsymbol{s}^T\boldsymbol{K}_D\boldsymbol{M}(\boldsymbol{q})^{-1}\left(\left(-\boldsymbol{C}(\boldsymbol{q},\dot{\boldsymbol{q}}) - \overline{\boldsymbol{C}}_D - \boldsymbol{C}_D^{'}\right)\boldsymbol{s} + \begin{bmatrix}\boldsymbol{F}_1\\ 0\end{bmatrix}\right) + \frac{1}{2}\boldsymbol{s}^T\dot{\boldsymbol{K}}_D\boldsymbol{s} = 0 \tag{2.15}$$

and

$$s^T\boldsymbol{K}_D\boldsymbol{M}(\boldsymbol{q})^{-1}\left(\left(-\boldsymbol{C}_D - \overline{\boldsymbol{K}}_D + \overline{\boldsymbol{C}}_D + \boldsymbol{C}_D^{'}\right)\boldsymbol{s} + \begin{bmatrix}\boldsymbol{F}_2\\ 0\end{bmatrix}\right) = -\boldsymbol{s}^T\boldsymbol{K}_v\boldsymbol{s}\ . \tag{2.16}$$

Notice that the sum of (2.15) and (2.16) is the same as the sum of (2.12) and (2.13).

Following the formulation presented in White et al. (2008), the vectors $\boldsymbol{F}_1$ and $\boldsymbol{F}_2$ are factored as

$$\boldsymbol{F}_i = \boldsymbol{F}_{im}\boldsymbol{s} \tag{2.17}$$

where the vector $\dot{\boldsymbol{q}}$ in White et al. (2008) has been replace with $\boldsymbol{s}$. Note that $\boldsymbol{F}_{im}$ in this factorization is an $m \times n$ real matrix. Using this factorization, the vector **s** can be stripped from either side of (2.15). However, in order for the scalar equation (2.15) to be true in the most general case, we must require the symmetric part of the resulting matrix equation to be zero. This realization leads the following requirement

$$\begin{aligned}&\dot{\boldsymbol{K}}_D - \boldsymbol{K}_D\boldsymbol{M}(\boldsymbol{q})^{-1}\left(\boldsymbol{C}(\boldsymbol{q},\dot{\boldsymbol{q}}) + \boldsymbol{C}_D'\right) - \left(\boldsymbol{C}(\boldsymbol{q},\dot{\boldsymbol{q}}) + \boldsymbol{C}_D'\right)^T \boldsymbol{M}(\boldsymbol{q})^{-1}\boldsymbol{K}_D \\ &+ \boldsymbol{K}_D\boldsymbol{M}(\boldsymbol{q})^{-1}\left(-\overline{\boldsymbol{C}}_D + \begin{bmatrix}\boldsymbol{F}_{1m}\\ 0\end{bmatrix}\right) + \left(-\overline{\boldsymbol{C}}_D + \begin{bmatrix}\boldsymbol{F}_{1m}\\ 0\end{bmatrix}\right)^T \boldsymbol{M}(\boldsymbol{q})^{-1}\boldsymbol{K}_D = 0.\end{aligned} \tag{2.18}$$

This is the same result as in White et al. (2008). The elements of $\boldsymbol{F}_{1m}$ and $\overline{\boldsymbol{C}}_D$ are chosen so that the last two terms of (2.18) will equal

$$\boldsymbol{K}_D\boldsymbol{M}(\boldsymbol{q})^{-1}\left(-\overline{\boldsymbol{C}}_D + \begin{bmatrix}\boldsymbol{F}_{1m}\\ 0\end{bmatrix}\right) + \left(-\overline{\boldsymbol{C}}_D + \begin{bmatrix}\boldsymbol{F}_{1m}\\ 0\end{bmatrix}\right)^T \boldsymbol{M}(\boldsymbol{q})^{-1}\boldsymbol{K}_D = -\beta\left(\boldsymbol{K}_D - \boldsymbol{K}_{Df}\right) \tag{2.19}$$

where β is a negative constant and $\boldsymbol{K}_{Df}$ is the final form of the matrix $\boldsymbol{K}_D$, i.e. the form that $\boldsymbol{K}_D$ attains when equilibrium is reached. In order to satisfy (2.19), $n(n+1)/2$ equations can be written to determine the same number of unknowns. In (2.19), there are a total of $n(n+1)/2 + nm$ unknowns in the matrices $\overline{\boldsymbol{C}}_D$ and $\boldsymbol{F}_{1m}$. The matrix $\overline{\boldsymbol{C}}_D$ can be used exclusively to solve (2.19), however there is some advantage in using both of the arrays $\overline{\boldsymbol{C}}_D$ and $\boldsymbol{F}_{1m}$ to solve (2.19). The reason for this will be discussed in consideration of the second matching equation.

Replacing the left hand side of (2.19) in (2.18) with the right hand side of (2.19) the first matching equation becomes

$$\dot{\boldsymbol{K}}_D - \boldsymbol{K}_D\boldsymbol{M}(\boldsymbol{q})^{-1}\left(\boldsymbol{C}(\boldsymbol{q},\dot{\boldsymbol{q}}) + \boldsymbol{C}_D'\right) - \left(\boldsymbol{C}(\boldsymbol{q},\dot{\boldsymbol{q}}) + \boldsymbol{C}_D'\right)^T \boldsymbol{M}(\boldsymbol{q})^{-1}\boldsymbol{K}_D - \beta\left(\boldsymbol{K}_D - \boldsymbol{K}_{Df}\right) = 0\,. \tag{2.20}$$

This set of ordinary differential equations is evaluated numerically as part of the feedback process. The matrix $\boldsymbol{C}_D'$ will be defined in the discussion of the second matching equation. A convenience of (2.20) is that by choosing β large and a path in which $\dot{\boldsymbol{q}}$ remains small, the matrix $\boldsymbol{K}_D$ remains relatively constant.

The Second Matching Equation

Again, using the factorization of (2.17) and stripping off the vector $\boldsymbol{s}$ from both sides of (2.16) produces the same equation as in White et al. (2008),

$$\boldsymbol{P}(t)\left(-\boldsymbol{C}_D - \overline{\boldsymbol{K}}_D + \overline{\boldsymbol{C}}_D + \boldsymbol{C}_D^{'}\right) + \boldsymbol{P}(t)\begin{bmatrix}\boldsymbol{F}_{2m}\\ 0\end{bmatrix} = -\boldsymbol{K}_v. \tag{2.21}$$

The matrix $\overline{\boldsymbol{C}}_D$ is already defined from the solution of the first matching equation and the sign of its eigenvalues are indeterminate, thus, $\boldsymbol{C}_D^{'}$ will be used to eliminate this term from the second matching equation and to provide additional "virtual damping" (see White et al. 2008) if desired. Given these definitions, note that all of the matrices $\overline{\boldsymbol{C}}_D$ and $\boldsymbol{C}_D^{'}$ together with the matrix $\boldsymbol{F}_{1m}$ all vanish as equilibrium is approached and the first matching equation shows the time derivative of $\boldsymbol{K}_D$ vanishes.

The solution of (2.21) involves the determination of the matrix $\boldsymbol{K}_v$ as well as the control law contribution $\boldsymbol{F}_{2m}$. A requirement of solving (2.21) is that $\boldsymbol{K}_v$ is symmetric and at least positive semi-definite. Should the four matrices in the parentheses in (2.21) be zero, then it is easy to see that $\boldsymbol{K}_v$ is not of full rank. Suppose the matrices $\overline{\boldsymbol{C}}_D$ and $\boldsymbol{C}_D^{'}$ are zero. Past examples in White et al. (2007, 2008) have shown that if the viscous damping coefficient matrix ($\boldsymbol{C}_D$) contributes positive damping on the un-actuated axes, then $\boldsymbol{K}_v$ will have positive eigenvalues. A useful illustration of this point is the ball and beam example shown in White, Foss and Guo (2007) where the damping on the un-actuated axis was contributed by the ball rubbing against a potentiometer sensor. However, should $\overline{\boldsymbol{C}}_D$ be nonzero then the nature of $\boldsymbol{K}_v$ is hard to determine since $\overline{\boldsymbol{C}}_D$ is based upon the difference of $\boldsymbol{K}_D$ and $\boldsymbol{K}_{Df}$. Because the matrix $\overline{\boldsymbol{C}}_D$ can cause difficulty in the controller performance, the first step in reducing the influence on the eigenvalues of $\boldsymbol{K}_v$ is to make $\overline{\boldsymbol{C}}_D$ as sparse as possible. Thus, when (2.11) is solved, the elements of $\boldsymbol{F}_{\boldsymbol{m}1}$ are used along with only those elements of $\overline{\boldsymbol{C}}_D$ necessary.

To solve (2.21), a two step process is used, the first step of which is

$$\begin{bmatrix}\boldsymbol{F}_{2m}\\ 0\end{bmatrix} = -\boldsymbol{P}(t)^{-1}\,\boldsymbol{K}_{v1} \tag{2.22}$$

for which the solution is

$$\boldsymbol{K}_{v1} = \sum_{i=1}^{m} \alpha_i \boldsymbol{P}_i \boldsymbol{P}_i^T \tag{2.23}$$

where the α_i are constants chosen so that $\boldsymbol{K}_{v1}$ is positive semi-definite and $\boldsymbol{P}_i$ is the i^{th} column of $\boldsymbol{P}(t)$. Applying (2.22) and (2.23) to (2.21) shows that

$$\boldsymbol{P}(t)\left(-\boldsymbol{C}_D - \overline{\boldsymbol{K}}_D + \overline{\boldsymbol{C}}_{\boldsymbol{D}} + \boldsymbol{C}'_{\boldsymbol{D}}\right) = -\boldsymbol{K}_{v2} \tag{2.24}$$

where $\boldsymbol{K}_v$ is defined as the sum of $\boldsymbol{K}_{v1}$ and $\boldsymbol{K}_{v2}$. The matrix $\overline{\boldsymbol{K}}_{\boldsymbol{D}}$ is defined as

$$\overline{\boldsymbol{K}}_{\boldsymbol{D}} = \gamma \boldsymbol{M}(\boldsymbol{q}) \tag{2.25}$$

where γ is a positive constant. The product of $\boldsymbol{P}(t)$ and the matrices in the parenthesis in (2.24) is not symmetric, however, the pre and post multiplication by $\boldsymbol{s}$ extracts the symmetric portion of the matrix product. With the matrix $\boldsymbol{C}'_{\boldsymbol{D}}$ defined as $\boldsymbol{C}'_{\boldsymbol{D}} \equiv -\overline{\boldsymbol{C}}_{\boldsymbol{D}}$, we must require

$$\frac{1}{2}\left[\boldsymbol{P}(t)\left(-\boldsymbol{C}_D - \overline{\boldsymbol{K}}_D\right) + \left(-\boldsymbol{C}_D - \overline{\boldsymbol{K}}_D\right)\boldsymbol{P}(t)^T\right] = -\boldsymbol{K}_{v2}\,. \tag{2.26}$$

Note that $\boldsymbol{F}_{2m}$ from (2.22) times the vector $\boldsymbol{s}$ provides the control signal $\boldsymbol{F}_2$. Because the matrices on the left of (2.25) are positive definite and symmetric, the resulting matrix sum

$$\boldsymbol{K}_v = \boldsymbol{K}_{v1} + \boldsymbol{K}_{v2} \tag{2.27}$$

is also symmetric and positive definite.

The Third Matching Equation

Stripping off the vector $\boldsymbol{s}$ from (2.14), we arrive at

$$\boldsymbol{K}_D \boldsymbol{M}^{-1}(\boldsymbol{q})\left(-\boldsymbol{G}(\boldsymbol{q}) + \begin{bmatrix} \boldsymbol{F}_3 \\ 0 \end{bmatrix} + \boldsymbol{P}(t)^{-1} \nabla \Phi(\boldsymbol{q})\right) = 0\,. \tag{2.28}$$

The solution procedure for (2.28) can be done in the same manner as shown in White et al. (2007). The remarkable result of this tracking controller development is that we have arrived at three matching equations that are (with the exception of $\overline{\boldsymbol{K}}_D$) identical to matching equations developed for stabilization as shown in White et al. (2006, 2007, 2008). However, it should be pointed out that control law (2.2) contains the sum of the vector containing $\boldsymbol{F}_3$ and the gradient of $\Phi(\boldsymbol{q})$. Upon examining (2.28) we see that this vector sum must be equal to $\boldsymbol{G}(\boldsymbol{q})$. The effect of this cancelation of non stable elements from the dynamic equations on the robustness of the closed loop system will be examined in the inverted pendulum cart example in Chapter 3.

Following The Path

The quantities involved in the evaluation of (2.6) require further explanation. The control law is given by (2.2) and the constraint that the lower $n - m$ elements of the actuation vector are zero is used to determine the vector $\boldsymbol{u}_2$. That the function $\Psi(\boldsymbol{s},\boldsymbol{u})$ is intended to be non-positive will be used to determine the vector $\boldsymbol{u}_1$.

The path following discussion will pertain to the case where the path motion constitutes a path that is contained in the solution space of the system. In order to have the system follow a prescribed trajectory, there are several possibilities. The first is to use the path information to determine the time histories of the generalized coordinates. By knowing the time histories of the coordinates (assumed to be sufficiently smooth) the generalized velocities and accelerations are also known. There are a total of n degrees of freedom and the path may specify either all or a subset of the generalized coordinates. If all coordinates are specified and the desired motion is possible given the underactuation, this represents one extreme in the classes of possible path following problems. At the other end, there is the situation where m coordinate histories are specified because fewer than m constraints may lead to redundant solutions. The m history constraints provide conditions to determine the m actuations. If m coordinate histories are specified, then the other n-m coordinate histories could be determined through inverse dynamics. In the general case, inverse dynamics is unattractive due to the time and complexity involved in the solution process. This complexity limits the ability of the system to respond rapidly to a given task. It should also be noted that in an underactuated system having m actuators, specifying m coordinate histories can in certain systems lead to redundant solutions for the other $n - m$ axes. This short discussion shows that there is a wealth of problem classes that can be considered.

Examples of three different classes of problems will be given in Chapters 3 and 4. In the ball and beam and inverted pendulum cart examples in Chapter 3, the number of specified coordinate histories equals the number of actuated axes. No inverse dynamics will be performed for those axes where the coordinate histories are not specified. However, one example in Chapter 5 with the rolling wheel will make use of inverse dynamics to determine all n coordinates to follow a figure eight shaped path. Given these classes of problems, there are four

subclasses that need to be considered. The first subclass includes those problems where the coordinate histories are specified for the unactuated axes. The second subclass involves those problems where the specified coordinate histories describe the motion of actuated axes. The third subclass consists of those problems were all n generalized coordinates have a specified coordinate history. A fourth subclass also exists for which some unactuated axes and some actuated axes have specified coordinate histories. An example of this type of implementation is given in Chapter 4.

In (2.6) it is assumed that m degrees of freedom have been specified, leaving $n - m$ coordinates unspecified. In (2.2), the lower $n - m$ equations are solved for the reference accelerations of the unspecified coordinates. This step is always possible because the mass/inertia matrix $\boldsymbol{M}(\boldsymbol{q})$ is of full rank. That the lower $n - m$ rows of (2.2) are equal to zero allows the reference accelerations to be found. In general, these $n - m$ equations are nonlinear and possibly unstable. The control $\boldsymbol{u}_2$ is used to stabilize these lower $n - m$ differential equations. How to best select $\boldsymbol{u}_2$ to stabilize these differential equations is a problem dependent exercise. Regardless of whether the solution of the lower $n - m$ equations is performed for actuated or non-actuated reference accelerations, the steps of the procedure are the same. Once the input vector $\boldsymbol{u}_2$ is determined, then $\boldsymbol{u}_1$ can be chosen to satisfy (2.9). If all n coordinates are specified, as in the first rolling wheel example presented in Chapter 4, then once the time histories and time derivatives are substituted into the lower $n - m$ equations, the vector $\boldsymbol{u}_2$ can be used to assure that the lower $n - m$ equations of (2.2) are all zero.

Removing the matching equations from (2.10), the remaining terms are

$$\boldsymbol{s}^T \boldsymbol{K}_D \boldsymbol{M}^{-1}(\boldsymbol{q}) \begin{bmatrix} \boldsymbol{u}_1 \\ \boldsymbol{u}_2 \end{bmatrix} = \Psi(\boldsymbol{s}, \boldsymbol{u}). \tag{2.29}$$

In order to satisfy Lyapunov, we desire that the right side of (2.28) is non-positive. This last relation completely defines the scalar function $\Psi(\boldsymbol{s},\boldsymbol{u})$. It is desired that the vector $\boldsymbol{u}_1$ in (2.29) be chosen so that Ψ is less than zero or at least the right hand side of (2.9) is non-positive. It will be shown that this is not always possible and the conditions for which (2.9) can be satisfied will be presented. If Ψ is to be other than positive, we must have

$$\boldsymbol{s}^T \boldsymbol{P}(t) \begin{bmatrix} \boldsymbol{u}_1 \\ \boldsymbol{u}_2 \end{bmatrix} \leq 0 \tag{2.30}$$

or if $\boldsymbol{P}(\boldsymbol{q})$ is partitioned as

$$\boldsymbol{P}(t) = \begin{bmatrix} \boldsymbol{P}_1 & \boldsymbol{P}_2 \end{bmatrix}, \tag{2.31}$$

we would then have

$$\boldsymbol{s}^T \boldsymbol{P}_1 \boldsymbol{u}_1 \le -\boldsymbol{s}^T \boldsymbol{P}_2 \boldsymbol{u}_2 . \tag{2.32}$$

Depending upon the dimension of $\boldsymbol{u}_1$, the ability to satisfy (2.30) might be limited. One possibility of satisfying (2.30) would be to determine $\boldsymbol{u}_1$ so that Ψ is zero. Experience has shown that this approach often results in a $\boldsymbol{u}_1$ vector that becomes extremely noisy as the vector $\boldsymbol{s}$ becomes small. Upon examining (2.2) it is seen that this noisy $\boldsymbol{u}_1$ is applied directly to the actuated states which can lead to undesirable system performance.

Instead of (2.30) a least squares approach is adopted in the determination of $\boldsymbol{u}_1$. We desire that

$$\begin{bmatrix} \boldsymbol{P}_1 & \boldsymbol{P}_2 \end{bmatrix} \begin{bmatrix} \boldsymbol{u}_1 \\ \boldsymbol{u}_2 \end{bmatrix} = -\boldsymbol{s} , \tag{2.33}$$

which can be rewritten as

$$\boldsymbol{P}_1 \boldsymbol{u}_1 = -\boldsymbol{s} - \boldsymbol{P}_2 \boldsymbol{u}_2 , \tag{2.34}$$

for which there are more equations than unknowns. Solving (2.34) in the least squares sense yields

$$\boldsymbol{u}_1 = -\left(\boldsymbol{P}_1^T \boldsymbol{P}_1\right)^{-1} \boldsymbol{P}_1^T \boldsymbol{s} - \left(\boldsymbol{P}_1^T \boldsymbol{P}_1\right)^{-1} \boldsymbol{P}_1^T \boldsymbol{P}_2 \boldsymbol{u}_2 . \tag{2.35}$$

This last relation provides a continuous dependence of $\boldsymbol{u}_1$ on $\boldsymbol{s}$ and $\boldsymbol{u}_2$. Equation (2.35) seems to work well with the exception of when $\boldsymbol{s}$ is orthogonal to the columns of $\boldsymbol{P}_1$, in which case Ψ becomes $-\boldsymbol{s}^T\boldsymbol{P}_2\boldsymbol{u}_2$, which may not remain negative.

In general, the control vector $\boldsymbol{u}$ will become zero as the system comes to rest, otherwise it will be nonzero. In equation (2.9), we see that the first term on the right hand side is quadratic in $\boldsymbol{s}$ and the second term is linear in $\boldsymbol{s}$. As $\boldsymbol{s}$ becomes small, it becomes increasingly difficult to assure that the sum of the two terms is non-positive. From this we see that there is a limit to our ability to ensure that the right hand side of (2.9) is negative as $\boldsymbol{s}$ becomes small. This implies that the norm of $\boldsymbol{s}$ will decrease until an ultimate bound is reached and once reached, will stay within this bound. It should be noted that once within this bound $\boldsymbol{s}$ cannot be guaranteed to decrease to zero. As seen in Lemma 2.1, this bound on $\boldsymbol{s}$ is a function of the eigenvalues of $\boldsymbol{K}_v$, $\boldsymbol{K}_D$, and the vector $\boldsymbol{u}$. For increased tracking accuracy this bound should be made as small as possible by the choice of $\boldsymbol{K}_D$, $\boldsymbol{K}_v$, and $\boldsymbol{u}_2$.

Lemma 2.1

From (2.6) the sliding mode dynamics are

$$\dot{\boldsymbol{s}} = \boldsymbol{M}^{-1}(\boldsymbol{q})\left(-\overline{\boldsymbol{K}}_D \boldsymbol{s} + \begin{bmatrix} \boldsymbol{u}_1 + \boldsymbol{F} \\ \boldsymbol{u}_2 \end{bmatrix} - \boldsymbol{C}(\boldsymbol{q},\dot{\boldsymbol{q}})\boldsymbol{s} - \boldsymbol{C}_D \boldsymbol{s} \right) \tag{2.36}$$

whose nominal form is

$$\dot{\boldsymbol{s}} = \boldsymbol{M}^{-1}(\boldsymbol{q})\left(-\overline{\boldsymbol{K}}_D \boldsymbol{s} + \begin{bmatrix} \boldsymbol{F} \\ 0 \end{bmatrix} - \boldsymbol{C}(\boldsymbol{q},\dot{\boldsymbol{q}})\boldsymbol{s} - \boldsymbol{C}_D \boldsymbol{s} \right). \tag{2.37}$$

Let $\boldsymbol{s}=\boldsymbol{0}$ be an exponentially stable equilibrium of the nominal system, and $L(t,\boldsymbol{s})$ be a Lyapunov function for the nominal system that satisfies (2.38-2.40). Suppose there exists positive constants c_1, c_2, c_3, and c_4 such that

$$c_1 \|\boldsymbol{s}\|^2 \le L(t,s) \le c_2 \|\boldsymbol{s}\|^2, \tag{2.38}$$

$$\dot{L} \le -c_3 \|\boldsymbol{s}\|^2, \tag{2.39}$$

$$\left\| \frac{\partial L}{\partial \boldsymbol{s}} \right\| \le c_4 \|\boldsymbol{s}\|, \tag{2.40}$$

and in $[0,\infty)$ x D, where $D=\{\boldsymbol{s}\in\Re^n \mid \|\boldsymbol{s}\|<\mathrm{r}\}$. Suppose the perturbation on the nominal system satisfies

$$\|\boldsymbol{g}(t,\boldsymbol{s})\| \equiv \left\| \boldsymbol{M}^{-1}(\boldsymbol{q})\left(\begin{bmatrix} \boldsymbol{u}_1 \\ \boldsymbol{u}_2 \end{bmatrix} \right) \right\| \le \delta < \frac{c_3}{c_4}\sqrt{\frac{c_1}{c_2}}\theta r \tag{2.41}$$

for all $t\ge 0$, all $\boldsymbol{s}\in D$, and some positive constant $\theta<1$. Then for all $\|\boldsymbol{s}(t_0)\| < \sqrt{\frac{c_1}{c_2}} r$, the solution of $\boldsymbol{s}(t)$ of the perturbed system (2.36) satisfies

$$\|\boldsymbol{s}(t)\| < \sqrt{\frac{c_2}{c_1}} e^{-\frac{(1-\theta)c_3}{2c_2}(t-t_0)} \|\boldsymbol{s}(t_o)\| \quad \forall\, t_o \le t \le t_o + T \tag{2.42}$$

and

$$\|\boldsymbol{s}(t)\| \le \frac{c_4}{c_3}\sqrt{\frac{c_2}{c_1}}\frac{\delta}{\theta}, \quad \forall t \ge t_o + T \tag{2.43}$$

for some finite time T.

Proof of Lemma 2.1

Using (2.7) as the candidate Lyapunov function for the nominal system (2.37-2.40) yield,

$$\lambda_{\min}\left(\boldsymbol{K_D}\right)\|\boldsymbol{s}\|^2 \le V(t,\boldsymbol{s}) = \frac{1}{2}\boldsymbol{s}^{\boldsymbol{T}}\boldsymbol{K_D}\boldsymbol{s} \le \|\boldsymbol{K_D}\|\|\boldsymbol{s}\|^2, \tag{2.44}$$

$$\dot{V} = -\boldsymbol{s}^{\boldsymbol{T}}\left(K_V\right)\boldsymbol{s} \le -\lambda_{\min}\left(\boldsymbol{K_V}\right)\|\boldsymbol{s}\|^2, \tag{2.45}$$

$$\left\|\frac{\partial V}{\partial \boldsymbol{s}}\right\| = \left\|\boldsymbol{K_D}\boldsymbol{s} + \boldsymbol{s}^T\frac{\partial \boldsymbol{K_D}}{\partial \boldsymbol{s}}\boldsymbol{s}\right\| \le \left\|\boldsymbol{K_D} + \boldsymbol{s}^T\frac{\partial \boldsymbol{K_D}}{\partial \boldsymbol{s}}\right\|\|\boldsymbol{s}\|. \tag{2.46}$$

If $\boldsymbol{K}_D$ remains virtually constant as in White et al. (2007, 2008) or if $\boldsymbol{s}$ remains small the last inequality can be approximated as

$$\left\|\frac{\partial V}{\partial s}\right\| \le \|\boldsymbol{K_D}\|\|\boldsymbol{s}\|. \tag{2.47}$$

For the perturbed system the candidate Lyapunov derivative (2.10) becomes

$$\begin{aligned}\dot{V} &= -\boldsymbol{s}^T\boldsymbol{K}_v\boldsymbol{s} + \Psi(\boldsymbol{s},\boldsymbol{u}) \le -c_3\|\boldsymbol{s}\|^2 + \left\|\frac{\partial V}{\partial \boldsymbol{s}}\right\|\|g(t,\boldsymbol{s})\| \\ &\le -c_3\|\boldsymbol{s}\|^2 + c_4\delta\|\boldsymbol{s}\| = -(1-\theta)c_3\|s\|^2 - \theta c_3\|s\|^2 + c_4\delta\|s\|, \quad 0<\theta<1 \\ &\le -(1-\theta)c_3\|s\|^2, \quad \forall\|s\| \ge \frac{\delta c_4}{\theta c_3}.\end{aligned} \tag{2.48}$$

Applying Theorem 4.18 of (Khalil, 2002) the ultimate bound is

$$B=\alpha_1^{-1}(\alpha_2(z)) \tag{2.49}$$

where

$$z = \frac{\delta c_4}{\theta c_3}, \tag{2.50}$$

$$\alpha_1(r) = \lambda_{\min}\left(\boldsymbol{K_D}\right)r^2, \tag{2.51}$$

$$\alpha_2(r) = \|\boldsymbol{K_D}\|r^2, \tag{2.52}$$

thus,

$$B = \sqrt{\frac{\|\boldsymbol{K_D}\|}{\lambda_{\min}\left(\boldsymbol{K_D}\right)}}\frac{\delta\|\boldsymbol{K_D}\|}{\theta\|\boldsymbol{K_V}\|}. \tag{2.53}$$

From this result we can see that the ultimate bound (B) depends on the magnitude of the perturbation $\|\boldsymbol{g}(t,\boldsymbol{s})\|$, the norm of matrices $\boldsymbol{K}_D$ and $\boldsymbol{K}_V$, and the minimum eigenvalue of $\boldsymbol{K}_D$.

Chapter Summary

In this chapter the development of the direct Lyapunov formulation for tracking control has been presented. There are two remarkable results of the tracking controller development. The first is that we arrived at three matching equations that are (with the exception of $\overline{\boldsymbol{K}}_D$) identical to matching equations developed for stabilization as shown in White et al. (2006, 2007, 2008). The second is that it is not necessary to perform inverse dynamics to specify every coordinate history to perform a system maneuver. Instead, the control law provides a means for determining the necessary unspecified coordinate histories. In addition a discussion on the expected performance of the tracking control scheme has been presented along with a lemma for estimating the ultimate bound on the norm of $\boldsymbol{s}$. This bound is a function of the eigenvalues of $\boldsymbol{K}_v$, $\boldsymbol{K}_D$, and the vector $\boldsymbol{u}$.

CHAPTER 3 - Holonomic Examples

In this chapter two examples of holonomic systems are presented. First, the inverted pendulum cart is presented and a desired trajectory is tracked with the actuated axis. The robustness of the control law in regards to system identification errors in $\boldsymbol{G}(\boldsymbol{q})$ is also discussed. Next, the ball and beam system is presented in which a desired trajectory is tracked with the ball, or unactuated axis. This chapter is concluded with a discussion on the observed performance of the tracking controllers for these two underactuated holonomic systems.

The Inverted Pendulum Cart

The inverted pendulum cart system is shown in Figure 3.1. The objective of the control law is to control the movement of the cart such that the pendulum remains upright while the cart tracks a desired path. The equations of motion for the system in the form of (2.1) are

$$\begin{bmatrix} \overline{m} & -\frac{ml}{2}\cos(\theta) \\ -\frac{ml}{2}\cos(\theta) & J \end{bmatrix}\begin{bmatrix} \ddot{x} \\ \ddot{\theta} \end{bmatrix} + \begin{bmatrix} 0 & \frac{ml}{2}\sin(\theta)\dot{\theta} \\ 0 & 0 \end{bmatrix}\begin{bmatrix} \dot{x} \\ \dot{\theta} \end{bmatrix} + \begin{bmatrix} 0 \\ -\frac{mgl}{2}\sin(\theta) \end{bmatrix} = \begin{bmatrix} F \\ 0 \end{bmatrix}, \qquad (3.1)$$

where m and l are the mass and length of the pendulum, respectively, $\overline{m}$ is the mass of the pendulum and cart, J is the mass moment of inertia of the pendulum about the pendulum base, and g is the acceleration of gravity. The state variables x and θ are as defined in Figure 3.1. The derivation of the dynamic equations for the examples presented in Chapter 3 and 4 are available for download at NLCLab.mne.ksu.edu (2007). The procedures outlined in Chapter 2 were followed to develop the DLA control law. Table 3.1 contains the system identification and the DLA controller parameters.

Table 3.1: Inverted Pendulum Cart Parameters

Quantity	Value	Quantity	Value
J	0.4 $Kg\ m^2$	a_1	.2 m
M	1.5 Kg	ω	.35 rad/s
$\overline{m}$	5.0 Kg	γ	1.0
L	0.7 m	α	1.0
G	9.81 m/s^2	β	-1000.0
$\boldsymbol{K}_{Df}$	$\begin{bmatrix} 200.0 & -300.0 \\ -300.0 & 550.0 \end{bmatrix}$	$\boldsymbol{\Lambda}$	$\begin{bmatrix} 0.1 & 0.0 \\ 0.0 & 1.0 \end{bmatrix}$

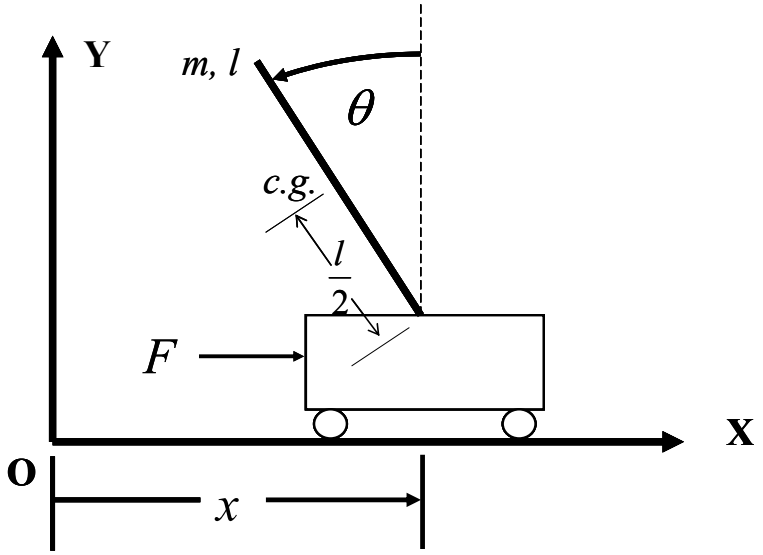

Figure 3.1: Inverted Pendulum Cart System

The desired x trajectory was defined as $x_d(t) \equiv a_1(1-\cos(\omega t))$. The desired pendulum angle was determined by solving for the second time derivative of θ from the lower $n - m$ rows of (2.2), then numerically integrating in time. This equation may be stable or unstable depending upon the system dynamics; however, the control law component $\boldsymbol{u}_2$ is meant to provide stabilization to the resulting matrix differential equation. For the inverted pendulum cart the resulting differential equation is unstable, thus $\boldsymbol{u}_2$ used to provide feedback linearization and was chosen as

$$\boldsymbol{u}_2 \equiv \frac{1}{2} ml\cos(\theta)\left(\ddot{x}_d - \lambda_1\left(\dot{x} - \dot{x}_d\right)\right) + \frac{1}{2} ml\sin(\theta) \\ \frac{1}{2}\gamma ml\cos(\theta)\left(\dot{x} - \dot{x}_d + \lambda_1\left(x - x_d\right)\right) + J\left(\gamma\left(\dot{\theta} - \dot{\theta}_d\right) + \lambda_2\dot{\theta}\right) \tag{3.2}$$

where λ_1 and λ_2 are the [1,1] and [2,2] elements of $\boldsymbol{\Lambda}$. In this example, the tracking of the cart position received a higher priority. This was accomplished by changing the relative magnitudes of λ_1 and λ_2 until the desired performance is obtained. How to best scale the relative weighting of λ_1 and λ_2 to achieve optimal tracking performance is an area of interest for future work. The control law component $\boldsymbol{u}_1$ was found through the evaluation of equation (2.35) and the matrix $\boldsymbol{K}_{Df}$ was chosen to be positive definite and symmetric.

The closed loop system response was simulated using MATLAB Simulink 7.5 for a period of 80 seconds. The initial position and velocity of the cart were set at zero. The pendulum position and velocity were initialized at 0 *rad* and 15 *rad/s,* respectively. Figure 3.2 shows the desired and actual cart position as a function of time. Figure 3.3 and Figure 3.4 show the desired and actual pendulum position and the sliding mode variables as a function of time respectively. The ultimate bound as defined in Lemma 2.1 and the norm of $\boldsymbol{s}$ ($\|\boldsymbol{s}\|$) are shown in Figure 3.5 and the constants used to calculate the ultimate bound are given in Table 3.2.

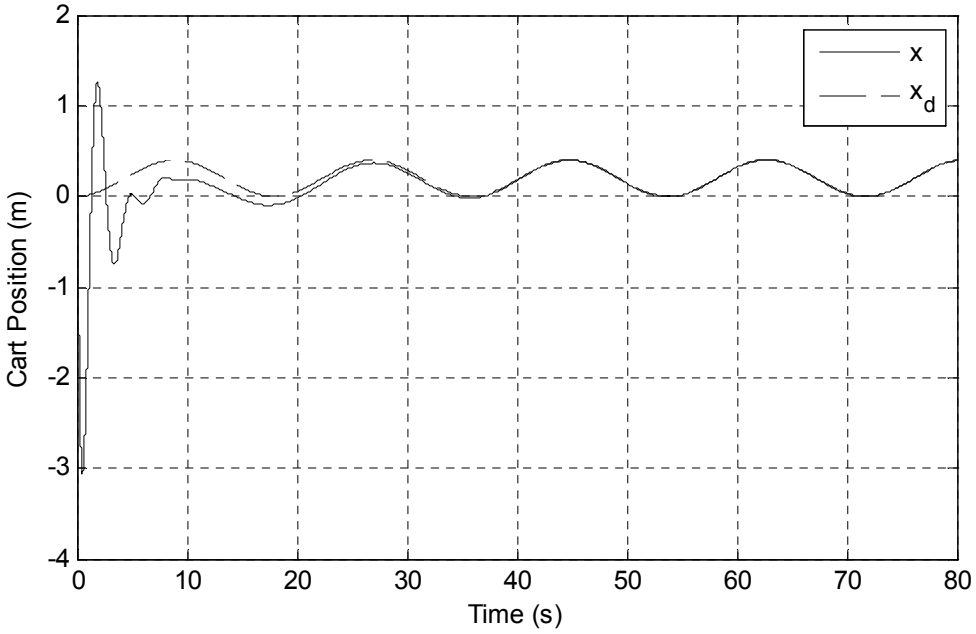

Figure 3.2: Desired and Actual Cart Position

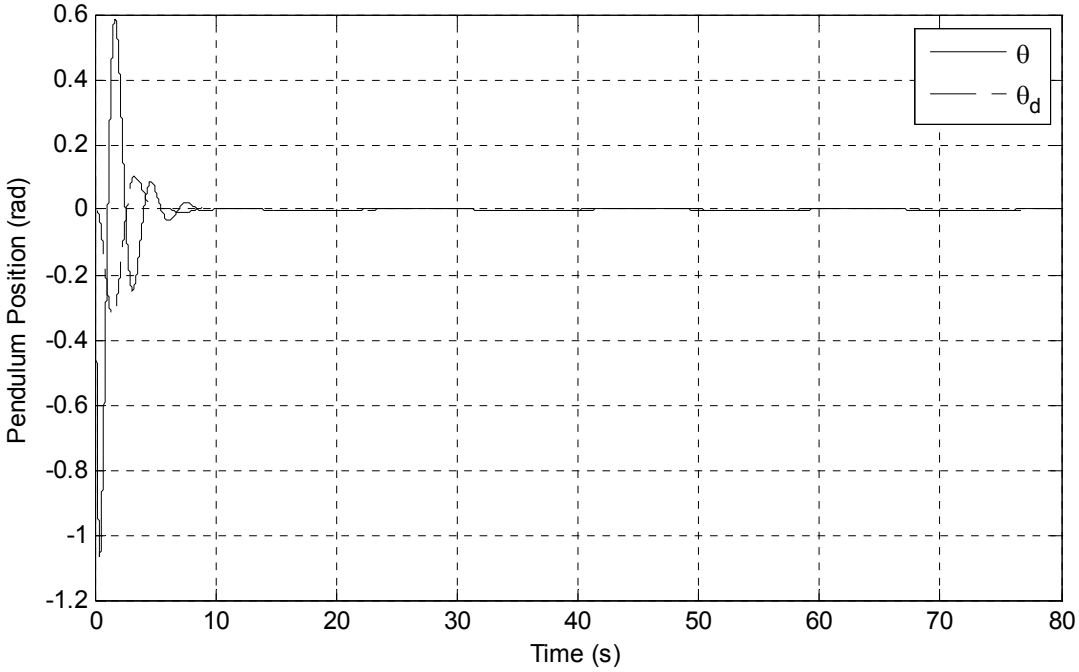

Figure 3.3: Desired and Actual Pendulum Position

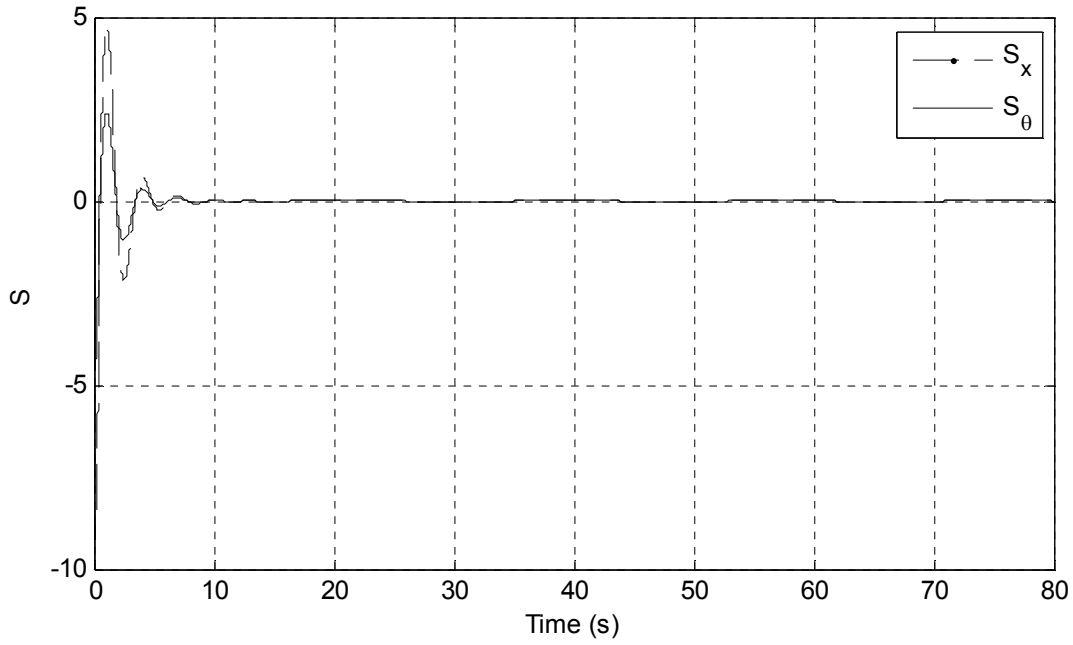

Figure 3.4: IP Cart *s* Time History

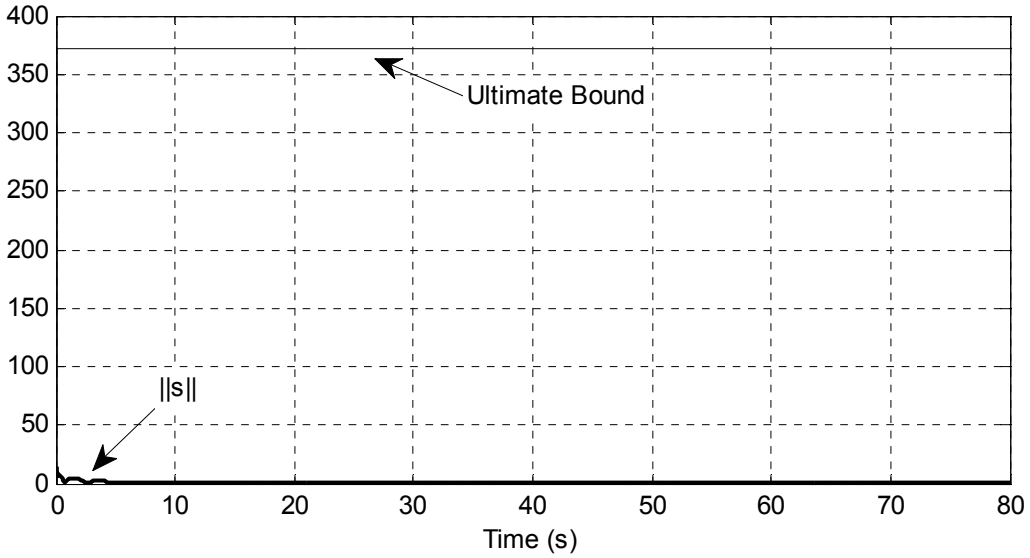

Figure 3.5: Time History of the Norm of *s*

Table 3.2: IP Cart Ultimate Bound Constants

Quantity	Value	Quantity	Value
r	408.5253	c_1	99.9962
θ	0.9993	c_2, c_4	750.1403
δ	23.3836	c_3	129.9686

From Figures 3.2-3.4 we see that the control law successfully rejects the initial disturbance and follows the desired trajectory on the actuated axis with minimal error. We can also see that the error on the pendulum axis seems to be greater than the cart tracking error. This supports the early statement concerning placing emphasis on the desired axis by adjusting $\boldsymbol{\Lambda}$.

Despite the good performance of the DLA tracking controller some questions still linger. Upon examining (2.6) and (2.27), we see that the control law is, in effect, canceling out the conservative field vector $\boldsymbol{G}(\boldsymbol{q})$. Because this vector was the cause of systems' instability, this raises questions about the robustness of such an approach when confronted with identification errors. In effect, will poor system identification with regards to terms contained in $\boldsymbol{G}(\boldsymbol{q})$ greatly degrade the control law performance?

In an effort to test the robustness of the closed loop system to this kind of identification error, 50 percent of the pendulum mass was added/subtracted to the system identification used in

the control law implementation. Additionally the desired position of the cart was set to zero. This results in a stabilization problem in the tracking sense. For this type of implementation we can test the robustness based upon the whether the cart can successfully reject a disturbance. If the cart can no longer return to the origin, or if its trajectories are greatly altered, by this type of error we can say that our controller is not robust to these types of errors.

The system response was simulated three times for a period of 60 seconds. In the first simulation the mass of the pendulum was the same in both the DLA implementation and the dynamic model. In the second and third, 50% of the mass was add and subtracted, respectively, from the DLA implementation but the mass in the dynamic model was kept the same. The initial cart position and velocities were zero. The pendulum position and velocity were initialized at zero and 15 *rad/s,* respectively. Figure 3.6 shows the desired and actual position of the generalized coordinate for a system with perfect identification and with the 50 percent added/subtracted from the pendulum mass. In comparing the response of the poorly indentified systems to response of the perfectly identified system in Figure 3.6 we can see that the DLA controller seems to be very robust to poor system identification of $\boldsymbol{G}(\boldsymbol{q})$. It is also apparent that the DLA controller is quiet robust to disturbances.

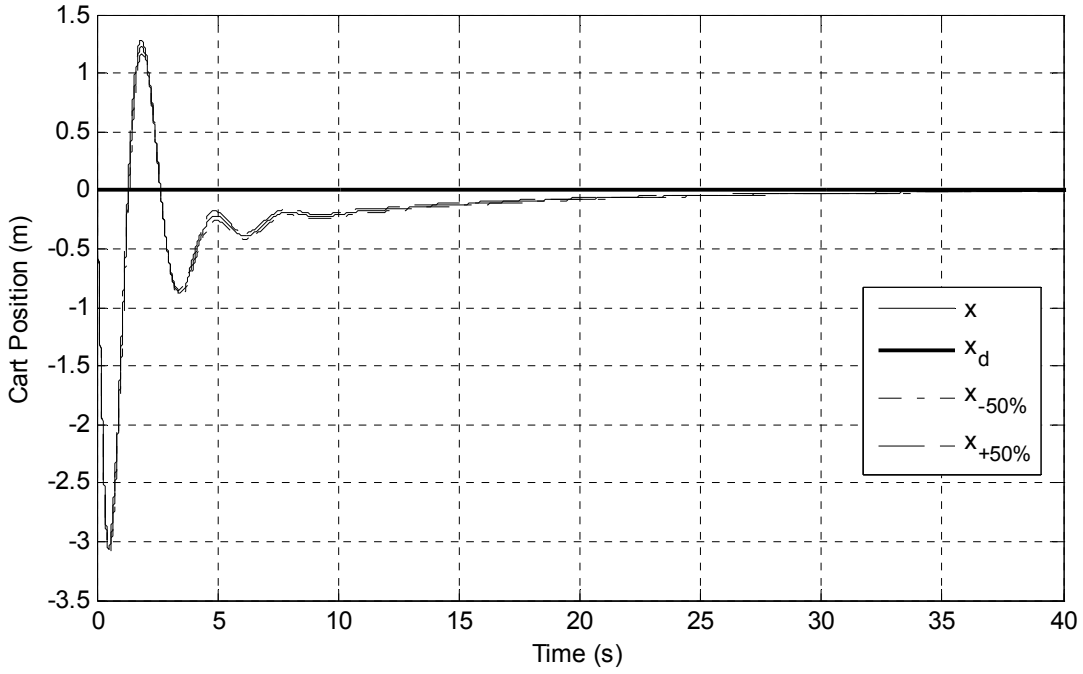

Figure 3.6: Perfect and Poor System ID Response

The Ball and Beam

Figure 3.7 shows the ball and beam system. The goal for the controller is for the unactuated axis, or ball position, to follow a desired path while maintaining a relatively small beam displacement angle. This contrasts with the inverted pendulum cart example for which the goal was to follow a desired path with the actuated axis, while stabilizing the unactuated one. The governing equations of motion are

$$\begin{bmatrix} \bar{I} + \frac{7}{5}mR_o^2 + mr^2 & -\frac{7}{5}mR_o \\ -\frac{7}{5}mR_o & \frac{7}{5}m \end{bmatrix} \begin{bmatrix} \ddot{\theta} \\ \ddot{r} \end{bmatrix} + \begin{bmatrix} r\,m\,\dot{r} & r\,m\,\dot{\theta} \\ -m\,r\,\dot{\theta} & C_d \end{bmatrix} \begin{bmatrix} \dot{\theta} \\ \dot{r} \end{bmatrix} + \begin{bmatrix} r\,mg\cos(\theta) - R_o mg\sin(\theta) \\ mg\sin(\theta) \end{bmatrix} = \begin{bmatrix} \tau \\ 0 \end{bmatrix} \tag{3.3}$$

where $\bar{I}$ is the mass moment of inertia of the beam, θ is the angle of inclination of the beam, r is the radial position of ball center relative to beam center, m is the mass of the ball, R_o is the radius of the ball, and C_d is the viscous damping coefficient of the rolling ball.

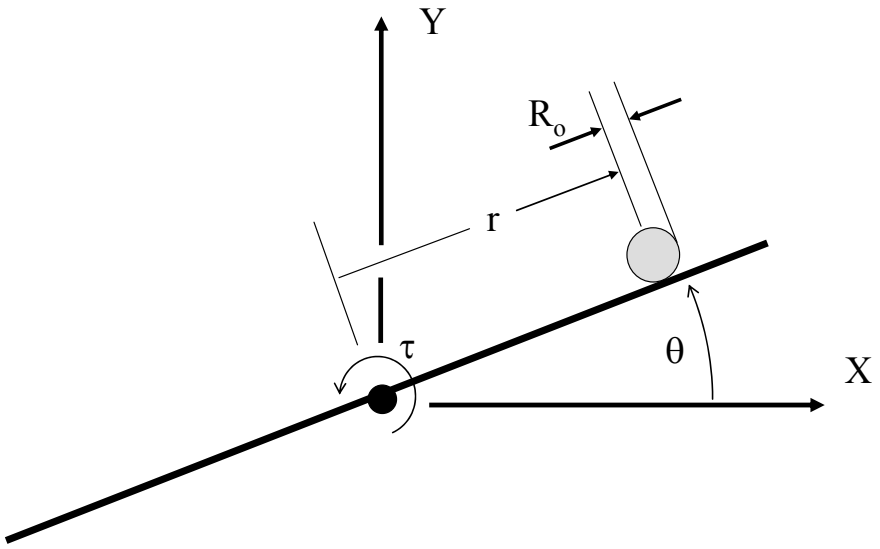

Figure 3.7: Ball and Beam System

Table 3.3: Ball and Beam Parameters

Quantity	Value	Quantity	Value
$\bar{I}$	0.4 $Kg\ m^2$	a_1	0.1 m
M	1.5 Kg	ω	0.3 rad/s
R_o	0.02 m	γ	0.0
C_d	0.16 $N\ s/m$	α	1.0
g	9.81 m/s^2	β	-1000.0
$\boldsymbol{\Lambda}$	$\begin{bmatrix} 0.05 & 0.0 \\ 0.0 & 2.0 \end{bmatrix}$	$\boldsymbol{K}_{Df}$	$\begin{bmatrix} 5.0 & -25.0 \\ -25.0 & 606.0 \end{bmatrix}$

Once again the formulation, as outlined in Chapter 2, was used to develop the DLA controller. Table 3.3 contains the system identification and controller parameters. For this example, the desired radial position of the ball, $r_d(t)$, was chosen as

$$r_d(t) \equiv a_1(1-\cos(\omega t)) + a_1 . \tag{3.4}$$

The desired beam angle was determined by numerically integrating in time the resulting differential equation from the lower *n-m* rows (2.2). The control law component $\boldsymbol{u}_2$ was chosen by feedback linearization to provide stabilization to this differential equation and is defined as

$$\boldsymbol{u}_2 \equiv -mg\sin(\theta) + mr\dot{\theta}\dot{\theta}_d + c_d(-\dot{r}_d + \lambda_2(r - r_d)) - \frac{7}{5}m(\ddot{r} - \lambda_2(\dot{r} - \dot{r}_d)) \tag{3.5}$$

where λ_2 is the [2,2] element of $\boldsymbol{\Lambda}$. The control law component $\boldsymbol{u}_1$ was found through the evaluation of equation (2.35). For the ball and beam example, $\mathbf{C}_D$ is nonzero on the unactuated axis, thus $\overline{\boldsymbol{K}}_D$ is not needed in equation (2.21) to insure the positive definiteness of $\boldsymbol{K}_v$. The matrix $\boldsymbol{K}_{Df}$ was chosen to be positive definite and symmetric.

The closed loop system response was simulated in Simulink for a period of 60 seconds. The initial position of the ball was chosen as 0.1 *m* and the initial angular velocity, angular position, and the ball velocity were set to zero. Figures 3.8 and 3.9 show the desired and actual ball and pendulum positions as a function of time, respectively. In comparing Figure 3.8 with Figure 3.9 we see that the chosen $\boldsymbol{\Lambda}$ allows for greater relative errors in the beam angle while having smaller errors in the ball position.

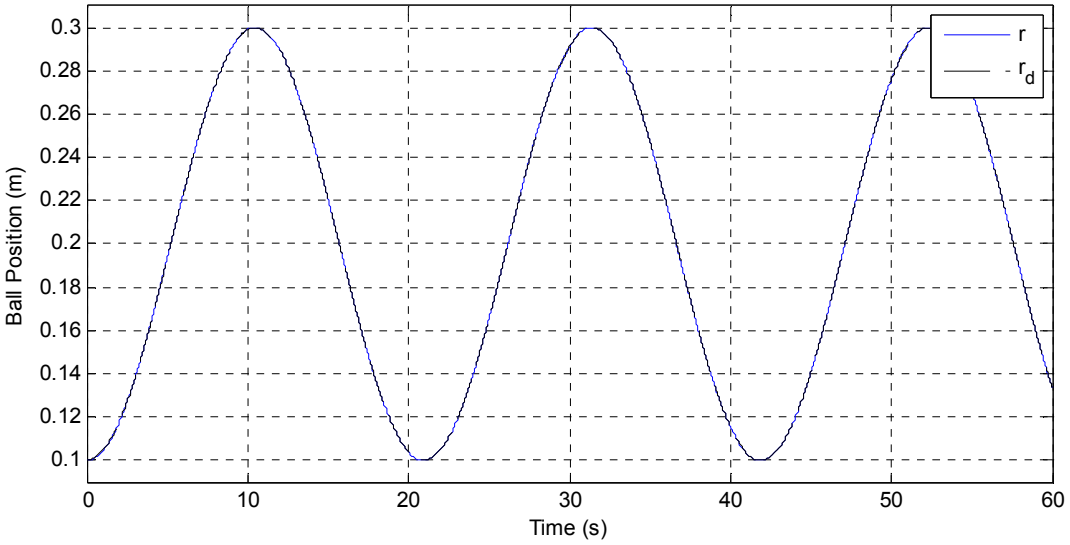

Figure 3.8: Desire and Actual Ball Position

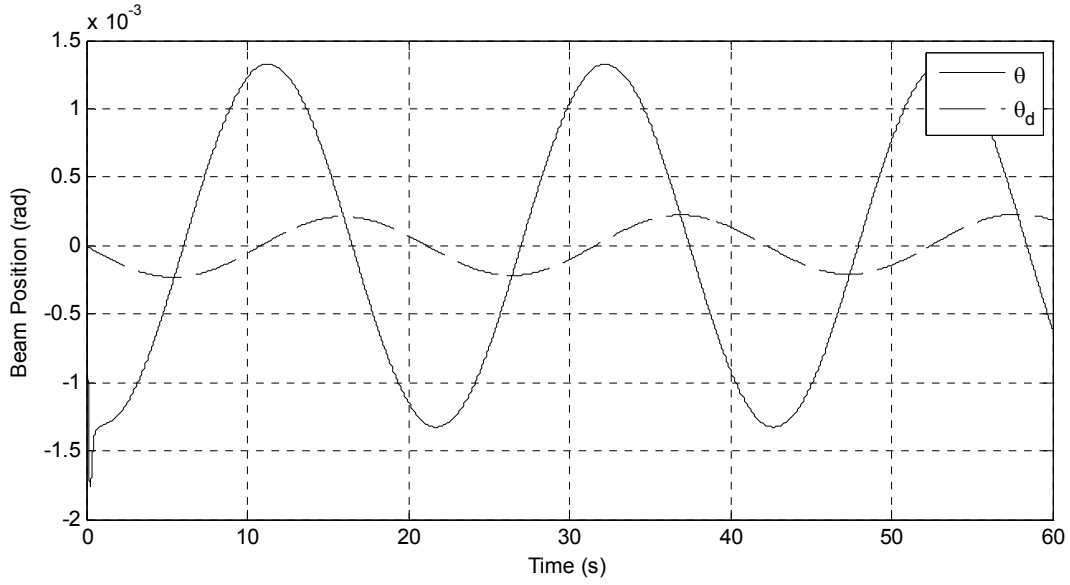

Figure 3.9: Desired and Actual Beam Angle

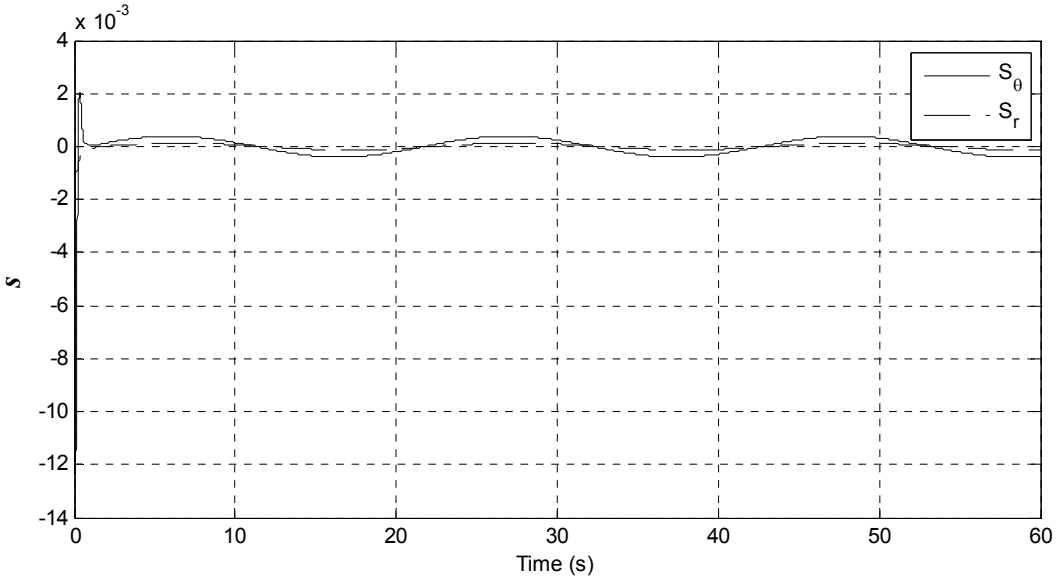

Figure 3.10: Ball and Beam *s* Time History

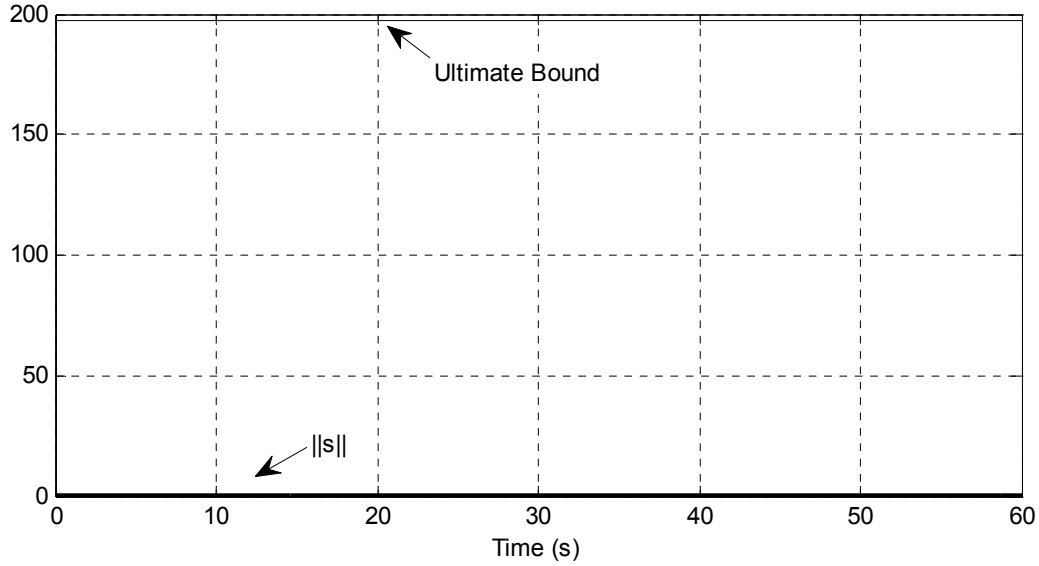

Figure 3.11: Ball and Beam ||*s*|| Time History

Figure 3.11 shows the time history of the ||***s***|| and the ultimate bound. The constants used to calculate the ultimate bound for this simulation are found in Table 3.4. It should be pointed out that the initial conditions of this simulation result in ***s*** equal to zero at t_0. The controller performance in tracking the desired trajectory as seen in Figure 3.8 is very good. The ||***s***||, as shown in Figure 3.11, remained well within the ultimate bound during the entire maneuver. In fact, upon examining Figures 3.5 and 3.11 we can see that the actual ||***s***|| for both examples is

much smaller than the estimate of the bound provided by Lemma 2.1. This suggests that Lemma 2.1 is too conservative. Determining a method of estimating the ultimate bound in a manner that is less conservative presents and interesting avenue for future work.

Table 3.4: Ball and Beam Ultimate Bound Constants

Quantity	Value	Quantity	Value
r	726.8972	c_1	3.9618
θ	0.9910	c_2, c_4	607.0432
δ	0.3917	c_3	4.1617

Chapter Summary

In this chapter the direct Lyapunov approach control scheme has been applied to several holonomic examples in contrasting manners. In the first example, the inverted pendulum cart, the desired path defined the coordinate history actuated axis and the lower *n-m* rows of equation (2.2) were used, in conjunction with $\boldsymbol{u}_2$, for the determination of the desired coordinate history unactuated axis. In the second example, the ball and beam, the unactuated coordinate history was specified by the desired path and the actuated coordinate history was determined from equation (2.2). The use of the control law (2.2), instead of inverse dynamics, to determine the desired coordinate histories for the unspecified axes represents a new and novel approach for the control of underactuated mechanical systems. The DLA controller performance is for the examples presented showed very good for tracking trajectories on the actuated axis (Figure 3.2), or on the unactuated axis (Figure 3.8). The direct Lyapunov approach for tracking control of underactuated mechanical systems has also been shown to work well in a system stabilization sense (Figure 3.6) and to be quiet robust to system identification errors and disturbances.

CHAPTER 4 - Nonholonomic Example

In this chapter the proposed control scheme is applied to a nonholonomic system. The rolling wheel example is presented and inverse dynamics are performed to determine the desired trajectories for the wheel to follow a figure eight shape in the X-Y plane. The desired trajectories are then tracked on both the actuated and unactuated axes. The robustness of the control law is discussed in regards to disturbance inputs and a comparison between feedforward and feedback control laws is provided. Additionally, an example of the controller implementation is presented in which one actuated and unactuated coordinate histories are defined by a desired path and (2.2) is used to determine the desired history of the other actuated axis. This chapter concludes with a discussion on the observed performance of the DLA tracking controller for this underactuated nonholonomic system.

The Rolling Wheel

Figure 4.1 shows the rolling wheel system. The system is setup in a similar way to the system described in Xu and Au (2004), where both θ (the wheel tilt) and ψ (the wheel rolling displacement angle) are actuated, thus leaving φ (the wheel orientation angle) as the unactuated coordinate. The goal for this example is to provide input torques that will roll the wheel in a figure eight shape in the X-Y plane. The dynamic equations of motion were found using (1.1) (NLCLab.mne.ksu.edu, 2007). The system was then reduced to a minimal set of generalized coordinates through the incorporation of holonomic and nonholonomic constraints (NLCLab.mne.ksu.edu, 2007).

The reduced system dynamic equations of motion are given in (4.1) where m is the mass of the wheel and R is the radius of the wheel. The variables ψ, θ, φ, τ_1, and τ_2 in equation (4.1) are all as denoted in Figure 4.1.

$$\begin{bmatrix} \frac{3}{2}mR^2 & 0 & \frac{3}{2}mR^2\sin(\theta) \\ 0 & \frac{5}{4}mR^2 & 0 \\ \frac{3}{2}mR^2\sin(\theta) & 0 & \frac{1}{4}mR^2\left(6-5\cos^2(\theta)\right) \end{bmatrix} \begin{bmatrix} \ddot{\psi} \\ \ddot{\theta} \\ \ddot{\varphi} \end{bmatrix} +$$

$$\begin{bmatrix} 0 & \frac{5}{2}mR^2\cos(\theta)\dot{\varphi} & 0 \\ 0 & 0 & -\frac{3}{2}mR^2\cos(\theta)\dot{\psi} - \frac{5}{4}mR^2\sin(\theta)\cos(\theta)\dot{\varphi} \\ 0 & \frac{1}{2}mR^2\cos(\theta)\left(\dot{\psi}+5\sin(\theta)\dot{\varphi}\right) & 0 \end{bmatrix} \begin{bmatrix} \dot{\psi} \\ \dot{\theta} \\ \dot{\varphi} \end{bmatrix} \qquad (4.1)$$

$$+\begin{bmatrix} 0 \\ -mgR\sin(\theta) \\ 0 \end{bmatrix} = \begin{bmatrix} \tau_1 \\ \tau_2 \\ 0 \end{bmatrix}.$$

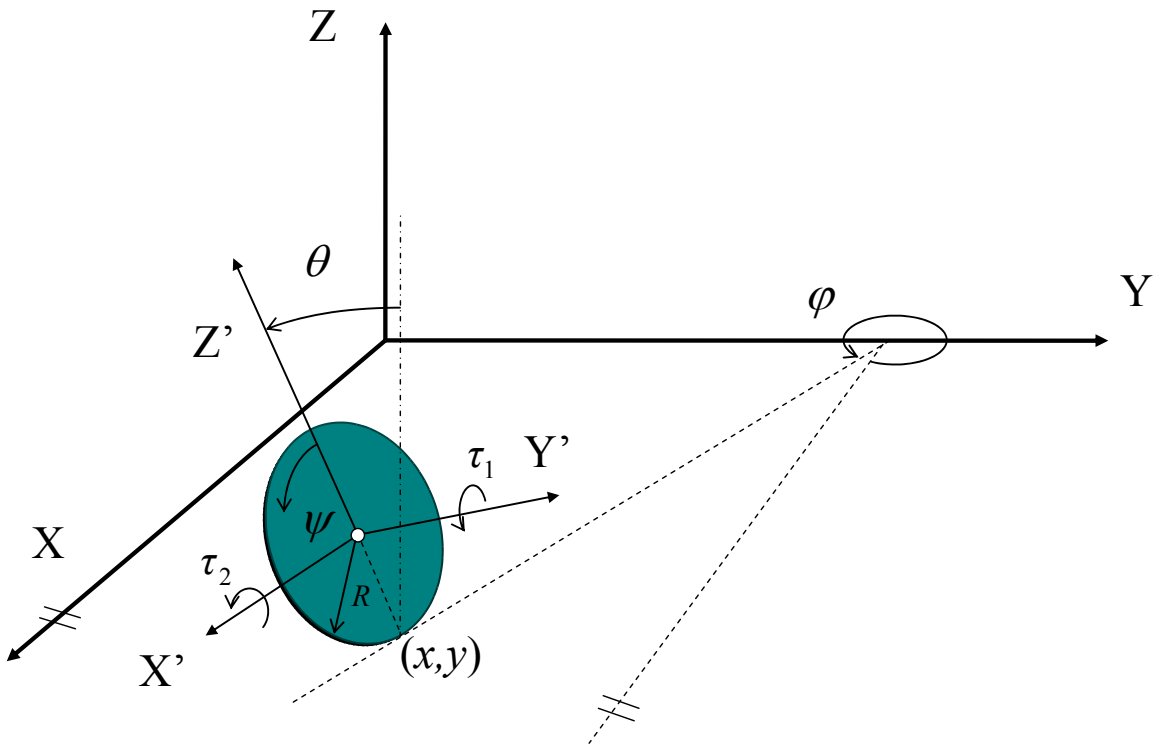

Figure 4.1: Rolling Wheel System

A rolling without slip assumption is made for the contact point (*x,y*), and inverse dynamics were performed to determine all of the desired state histories. While inverse dynamics were not a necessity of implementing the control law (2.2), it was required for a comparison of

feed forward and feedback based control laws presented later. The desired coordinate histories of ψ, and φ were determined from the nonholonomic constraints,

$$\dot{x} - R\cos(\varphi)\dot{\psi} = 0\,, \tag{4.2}$$

and

$$\dot{y} - R\sin(\varphi)\dot{\psi} = 0\,. \tag{4.3}$$

From equations (4.2) and (4.3) we get

$$\varphi_d = \tan^{-1}\left(\frac{\dot{y}_d}{\dot{x}_d}\right), \tag{4.4}$$

and

$$\dot{\psi}_d = \frac{\dot{x}_d\cos(\varphi_d) + \dot{y}_d\sin(\varphi_d)}{R}, \tag{4.5}$$

Fore the desired trajectories. The desired coordinate history for θ was determined by differentiating the last row of (4.1), solving for the second time derivative of θ, and then numerically integrating the resulting differential equation in time.

The desired motion in the X-Y plane as a function of time was chosen as the solution of

$$x_d^4(t) = r^2\left(x_d^2(t) - y_d^2(t)\right), \tag{4.6}$$

where

$$x_d(t) \equiv r\sin(\omega t), \tag{4.7}$$

r is the maximum desired x position, and ω is the angular frequency of oscillation in *rad/s*. The system identification along with the controller parameters are found in Table 4.1.

Table 4.1: Rolling Wheel System Parameters

Quantity	Value	Quantity	Value
M	5.0 *Kg*	R	0.5 *m*
G	9.81 m/s^2	β	-100.0
r	10.0 *m*	ω	0.5 *rad/s*
γ	0.75	α	1.0
$\boldsymbol{K}_{Df}$	$\begin{bmatrix} 20.0 & -1.0 & -3.0 \\ -1.0 & 20.0 & 1.0 \\ -3.0 & 1.0 & 2.0 \end{bmatrix}$	$\boldsymbol{\Lambda}$	$\begin{bmatrix} 1.0 & 0.0 & 0.0 \\ 0.0 & 1.0 & 0.0 \\ 0.0 & 0.0 & 10.0 \end{bmatrix}$

The closed loop system response was simulated for a period of 14 seconds with Simulink. All of the states were initialized to zero with the exception of $\dot{\psi}(0) = 14.1421$ *rad/s*, $\dot{\theta}(0) = 0.0531$ *rad/s*, and $\varphi(0) = 0.7854$ *rad*. Figure 4.2 shows the desired and actual position of the wheel contact point. Figures 4.3-4.5 show the desired and actual orientation angles as a function of time. The matrix $\boldsymbol{K}_{Df}$ was chosen to be positive definite and symmetric. Because all of the coordinate histories were specified by the inverse dynamics the control law component $\boldsymbol{u}_2$ was not needed for stabilization and, thus, it was chosen to ensure that the right had side of the lower *n-m* rows of (2.2) were zero and the control law component $\boldsymbol{u}_1$ was determined from the solution to (2.35).

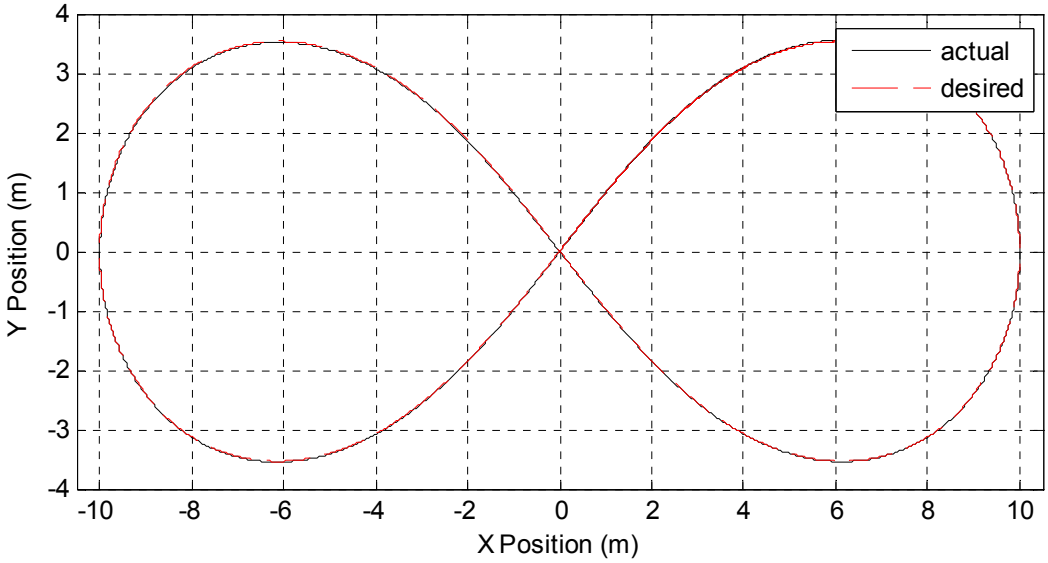

Figure 4.2: Rolling Wheel Trajectory X-Y Plane

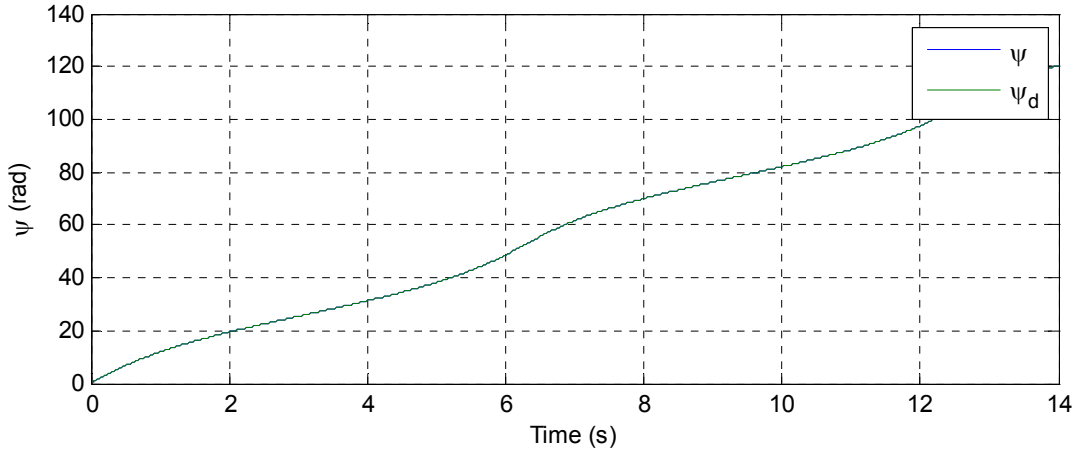

Figure 4.3: Actual and Desired ψ

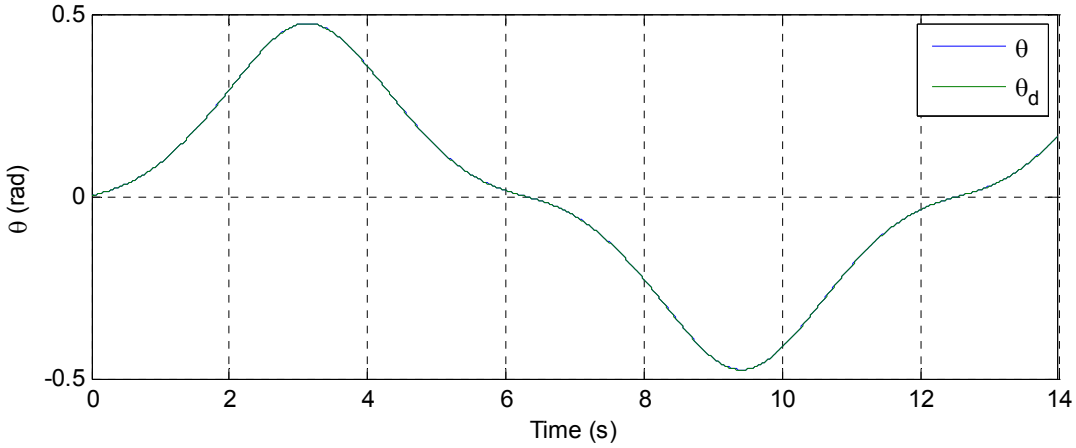

Figure 4.4: Actual and Desired θ

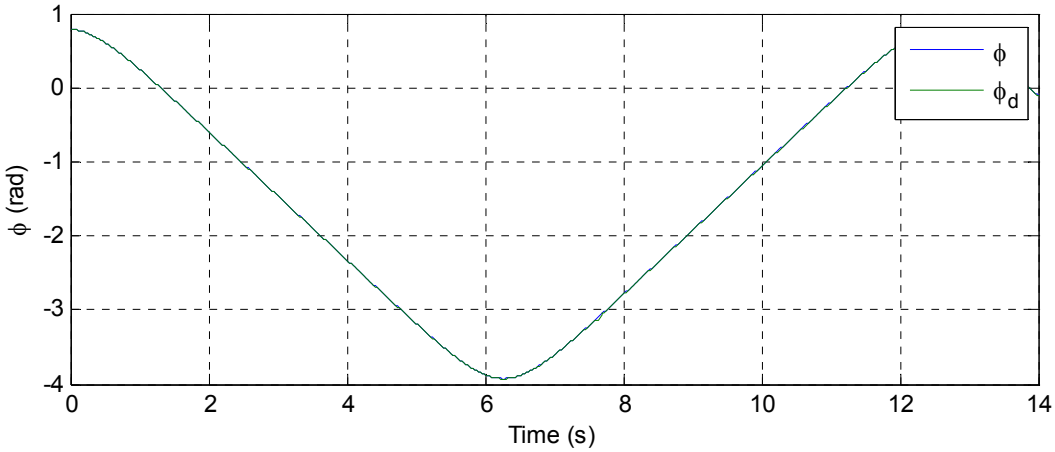

Figure 4.5: Actual and Desired φ

From Figures 4.2 - 4.5, we see that the controller tracks the desired trajectories on all axes with very little error. Since the control law performs admirably without disturbances it raises the following questions: What will happen when a disturbance is introduced? Will the controller be able to successfully reject this disturbance and track the desired coordinates? Also, since we are already doing inverse dynamics why do we need to design a feedback control law? Couldn't the dynamic equations be used to determine the necessary torques to follow the path? Also, is it possible to use to use the last equation from (2.2) to determine the θ desired without the use of inverse dynamics?

Feed Forward vs. Feed Back

To answer the first three questions the previous example was modified to add a step disturbance on the ψ axis. The simulated response of the system of was then compared to a system utilizing a feed forward control scheme. The feed forward control signal was found by substitution of the desired coordinate histories into the dynamic equations (4.1) and then evaluating the resulting input torques. Figures 4.6- 4.9 illustrate the effect of the disturbance of 1.0 N-m from 1 to1.5 seconds on both systems.

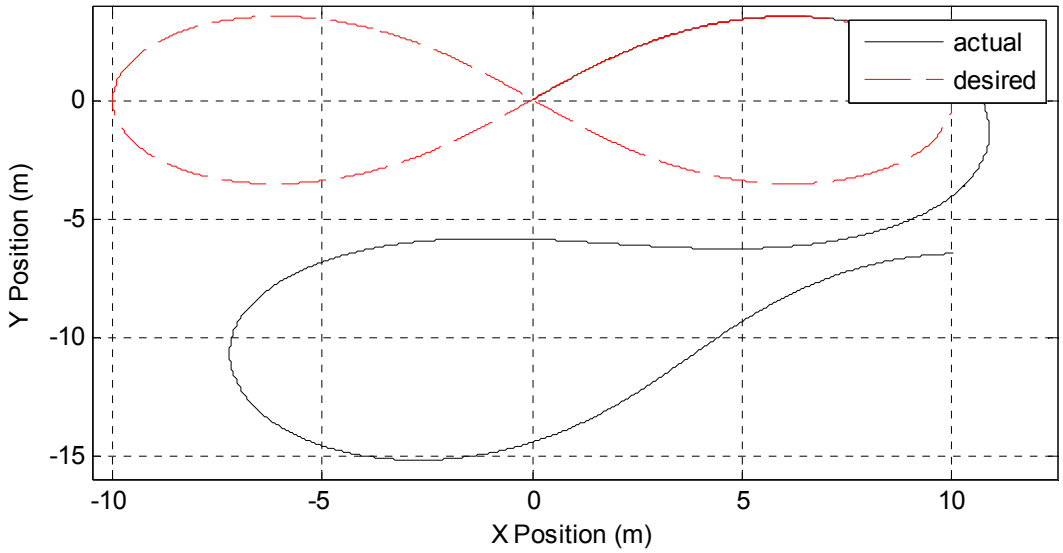

Figure 4.6: RW Trajectory-Feed Forward Control with Disturbance

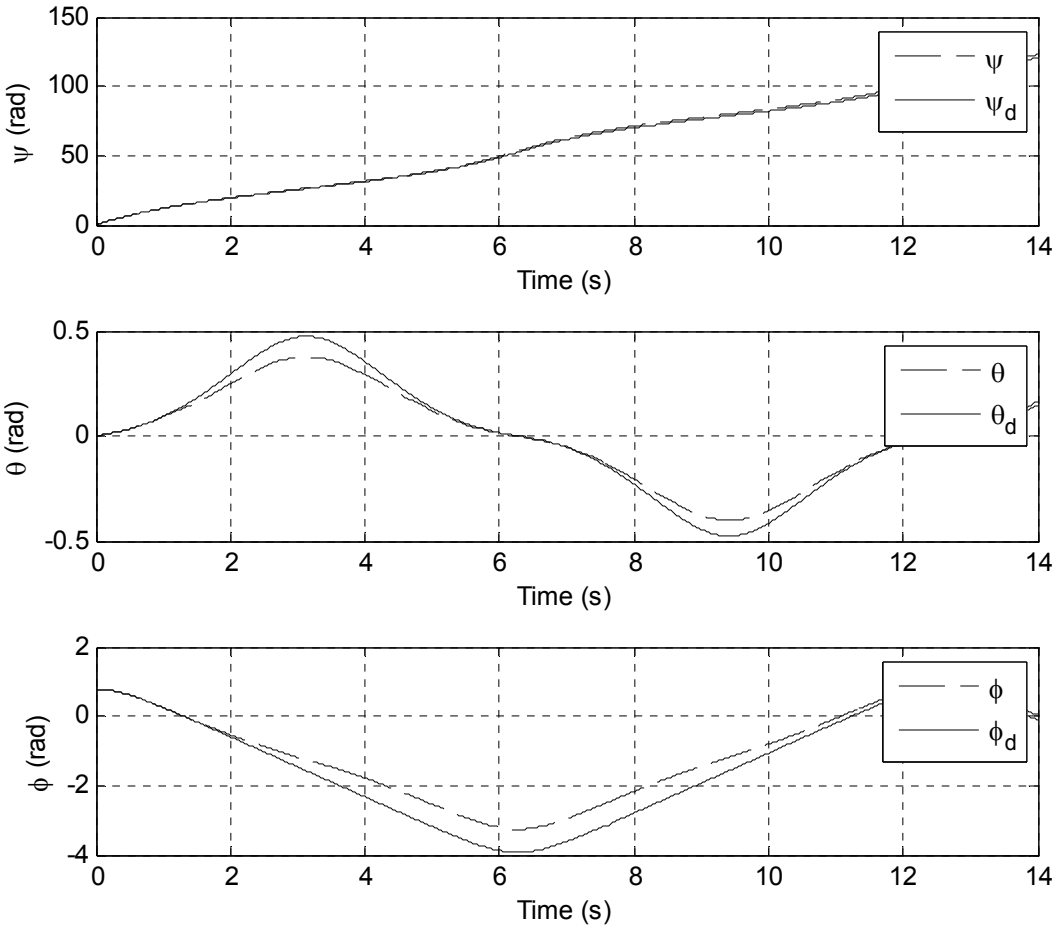

Figure 4.7: Orientation Angles-Feed Forward Control with Disturbance

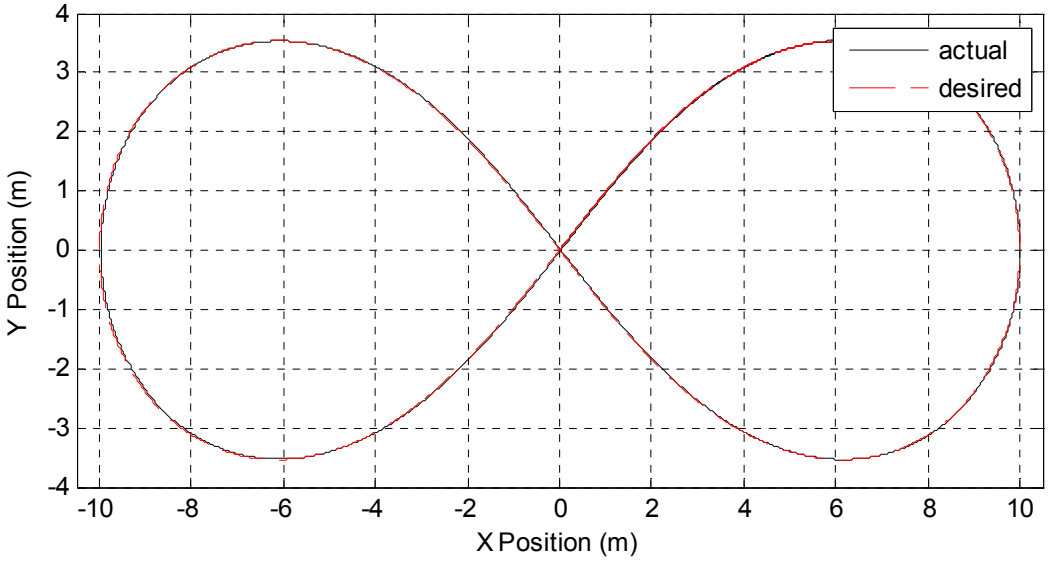

Figure 4.8: RW Trajectory-Feedback with Disturbance

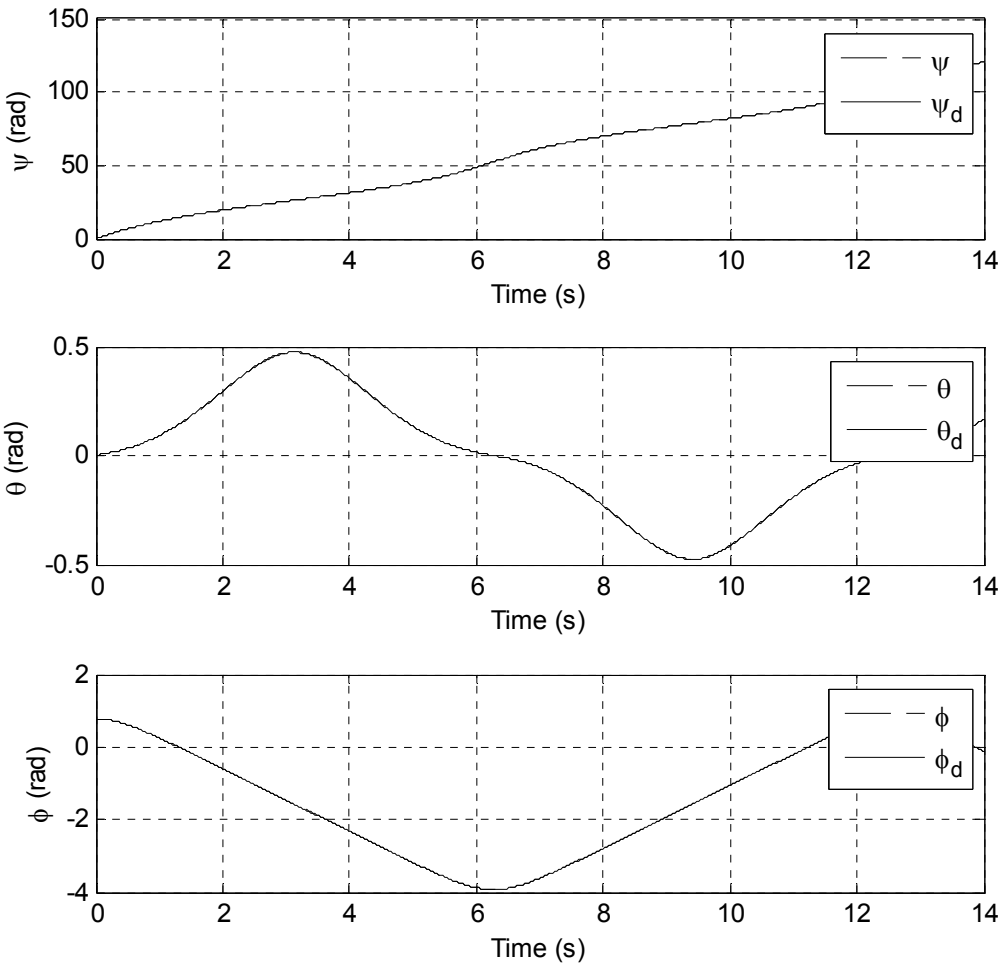

Figure 4.9: Orientation Angles-Feedback with Disturbance

In comparing Figures 4.6-4.7 to Figures 4.8-4.9 we can see that even a small disturbance can significantly alter the trajectory of the feed forward system. The feedback controlled system, however, is able to successfully reject this disturbance and continue tracking the desired trajectories with very little error. Since the feedback control law using inverse dynamics to develop the desired θ time history has been shown to reject disturbances, let us now address the question of whether it is necessary to perform the inverse dynamic calculations to determine θ_d .

Upon examining (4.1) and (2.2) you may notice that our previous strategies of solving the n-m rows of (2.2) for $\ddot{\theta}$ will not work because $\ddot{\theta}_d$ does not appear in the last row of (2.2). Unfortunately, it must be determined because it is required for the control law calculation. To address this problem, solve the last row of (2.2) for $\dot{\theta}_d$ and then numerically integrated the

resulting differential equation. Because $\ddot{\theta}_d$ is only used in the DLA control law in one place, a backward, first order finite difference method ($\ddot{\theta}_d = \frac{\Delta\dot{\theta}_d}{\Delta t}$) was used to estimate $\ddot{\theta}_d$.

For this example the desired ψ and φ histories were the same as the previous examples. Since (2.2) was used to develop θ_d, the last equation of (2.2) should be satisfied, thus $\boldsymbol{u}_2$ and $\boldsymbol{u}_1$ were set to zero. It should be pointed out that if both $\boldsymbol{u}_1$ and $\boldsymbol{u}_2$ are zero, the feedback controlled system becomes the nominal system denoted in equation 2.37. Provided that we satisfy all of the matching equations, the tracking error vector ($\boldsymbol{s}$) should be exponentially stable. However, the use of the difference method to estimate the desired acceleration on the θ axis introduces a small amount of error in the solution to the matching equations.

The closed loop system response was simulated for a period of 14 seconds in Simulink. The same disturbance in the previous examples was applied to the ψ axis. Figure 4.10 illustrates the desired and actual path in the X-Y plane that the wheel followed. Figure 4.11 shows the desired and actual orientation angles of the rolling wheel system during the maneuver. From this figure we see that the performance of the controller is excellent. The disturbance does not seem to cause any deviation from the desired orientation angles and as a result the wheel tracks the desired trajectory in the X-Y plane.

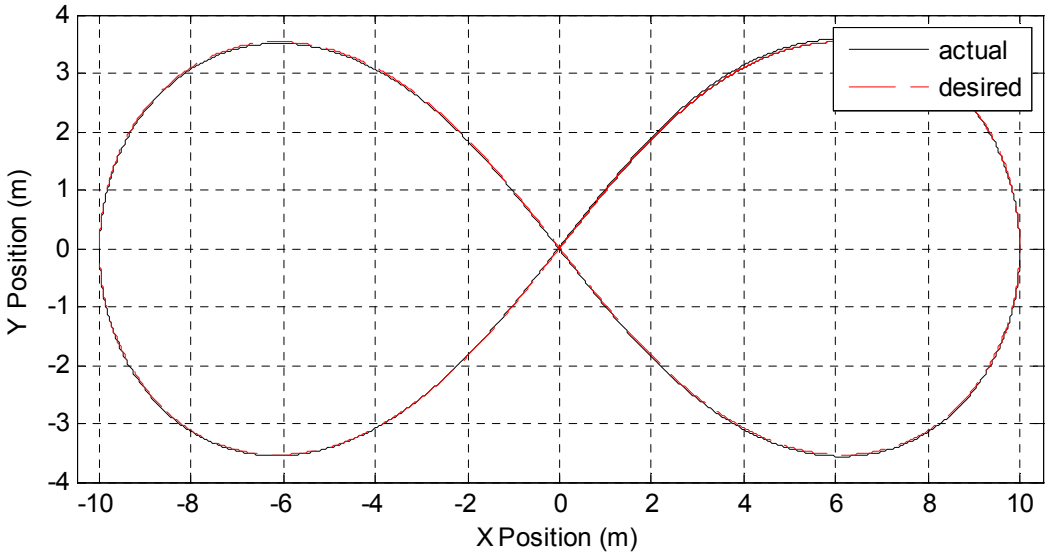

Figure 4.10: RW Trajectory-Feedback without Inverse Dynamics

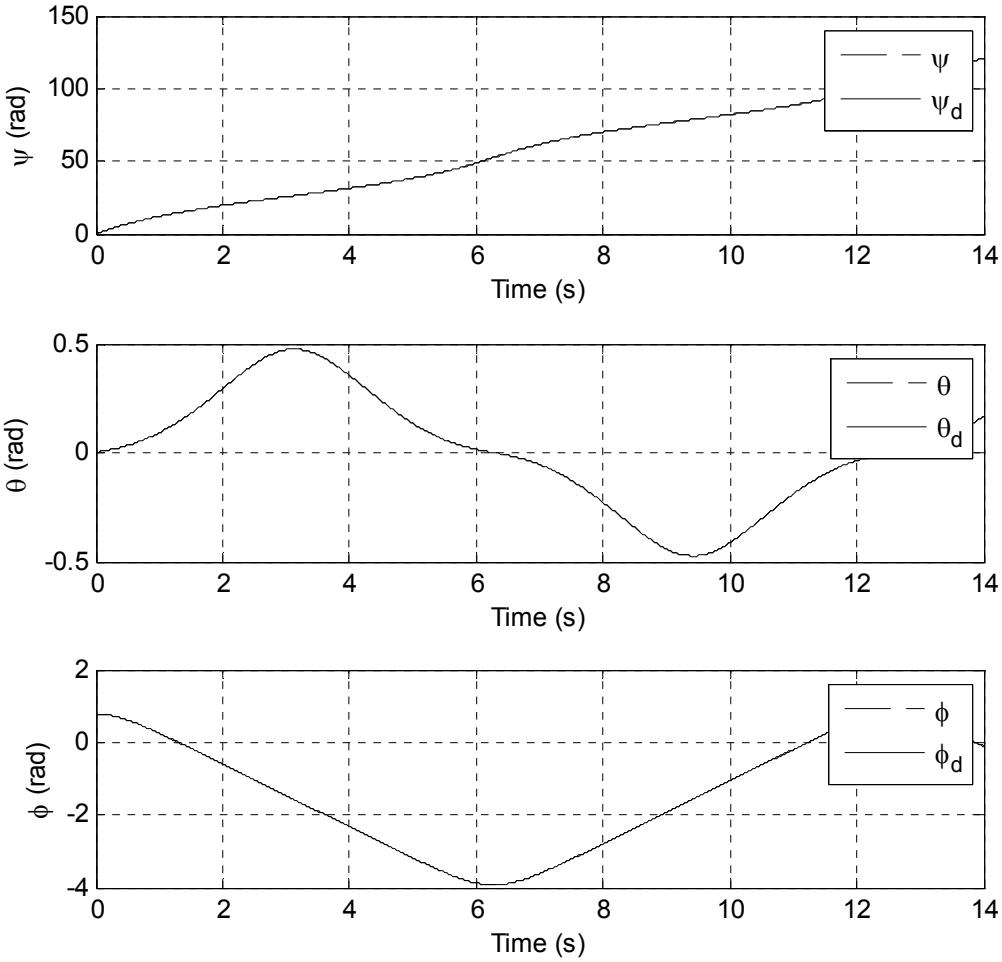

Figure 4.11: Orientation Angles-Feedback without Inverse Dynamics

It should also be noted that the desired trajectory calculations are open loop with respect to the *x* and *y* coordinates. It is possible that the feedback controlled system could recover from a disturbance in the sense of the orientation angles but not return to the desired X-Y path. Figures 4.12 and 4.13 illustrate an example of just such a case in which the φ was initialized to zero. In order to handle such disturbances it is suggested that either, the system model should not be reduced beyond the five degrees of freedom model that contains the three orientation angles and the *x* and *y* position of the contact point, or that a navigator be developed that would use the current position to modify the desired orientation angles in order for the system to return to the desired trajectory. The question of which approach would yield better performance is an area of interest for future research.

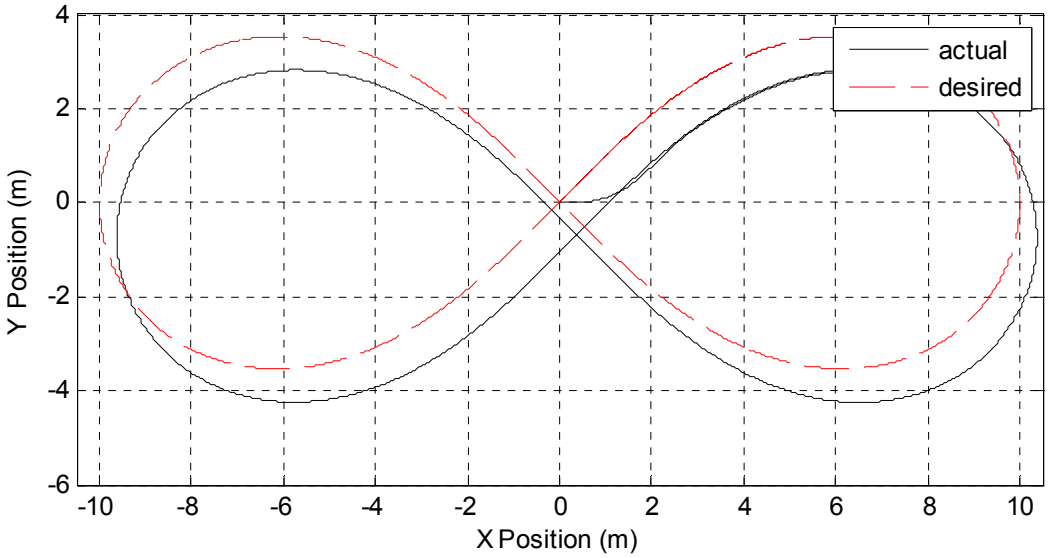

Figure 4.12: RW Trajectory-Initial Orientation Error

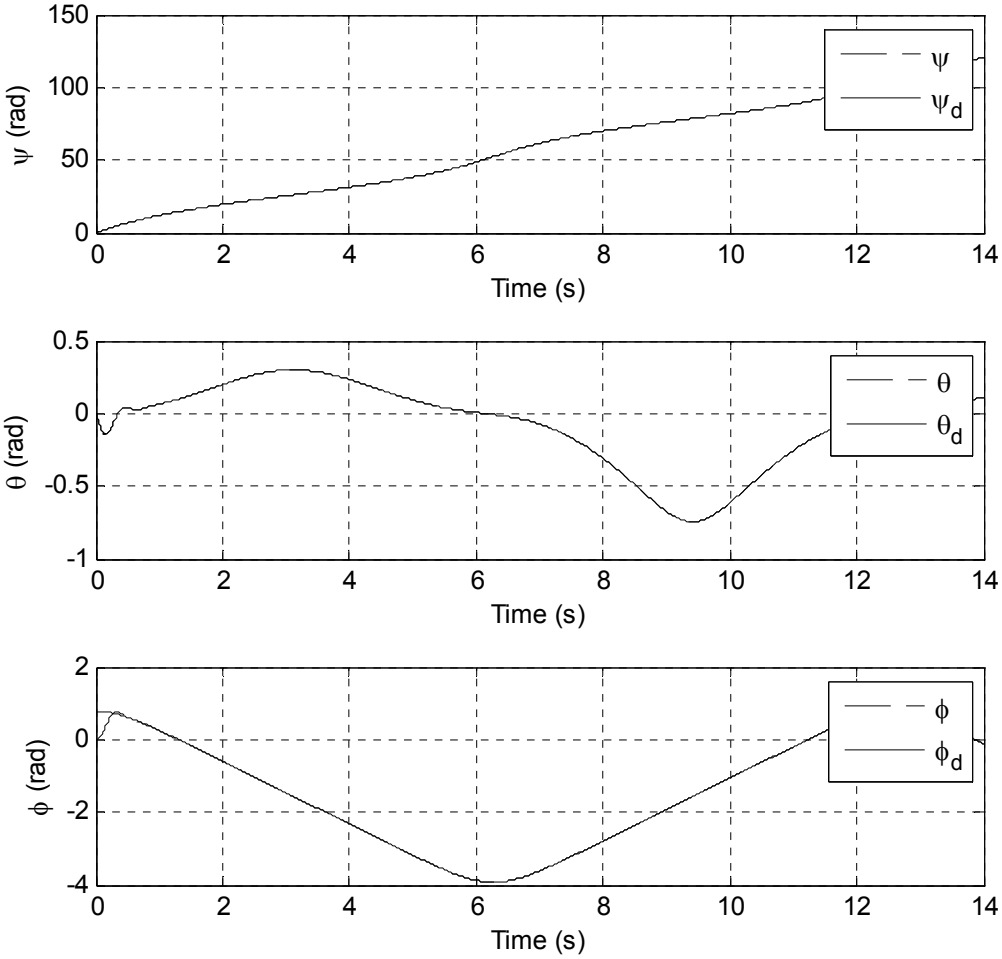

Figure 4.13: Orientation Angles-Initial Orientation Error

Chapter Summary

In this chapter an example of a nonholonomic system, the rolling wheel, was presented. A feedback control law was developed using the direct Lyapunov approach. The determination of the desired coordinate histories was determined in two contrasting ways. In the first, inverse dynamics and the desired path were used to determine the θ_d time history. In the second, the lower *n-m* equations of equation (2.2) were used to solve for the $\dot{\theta}_d$, then the resulting equation was numerically integrated to determine θ_d. The desired acceleration on this axis was estimated using a backwards, first order finite difference technique. The control law was shown to be robust in regards to step disturbance inputs and initial condition errors. With the completion of this example the performance of the direct Lyapunov controller has been shown to be very good for both holonomic and nonholonomic system in simulation.

CHAPTER 5 - Inverted Pendulum Cart Implementation

In this chapter the proposed direct Lyapunov approach control scheme is applied to a real inverted pendulum cart system. The dynamic model is derived using first principles and system identification is performed to determine certain coefficients in the dynamic model. The DLA control scheme is applied to the real system and the positions of the cart and pendulum recorded. Finally, this chapter is concluded with a discussion on the observed performance of the tracking controller and some recommendations are provided which may improve the controller performance.

The Inverted Pendulum Cart Model

In Chapter 3, the model for the inverted pendulum cart (IP cart) merely assumed that a force was applied to the cart, however, in a real world system that force must actually be applied. To apply this input force to the cart, the laboratory inverted pendulum cart system makes use of a DC motor, drive chain, and several sprockets. This necessarily complicates the dynamic model of the system due to the chain tension and back EMF of the motor. It also changes the control input from a force to a voltage that is applied to the motor.

Figure 5.1 contains the free body diagrams of each element the IP cart system. The dynamic model is derived using a Newton-Euler approach. Starting with the pendulum the Newton-Euler equations are

$$-A_x = m_p \ddot{x}_p, \tag{5.1}$$

$$-A_y - m_p g = m_p \ddot{y}_p, \tag{5.2}$$

and

$$\frac{m_p g l \sin(\theta)}{2} = I_p \ddot{\theta}, \tag{5.3}$$

where $I_p = m_p l^2/3$.

Assuming that the cart stays firmly on the ground, with no vertical movement, the Newton-Euler equations for the cart are

$$A_x + B_x + C_x + F_x = m_c \ddot{x}_c, \tag{5.4}$$

$$A_y + B_y + C_y + F_y - m_c g = 0\,, \tag{5.6}$$

and

$$-\tau_m + (C_y - B_y)d_4 - A_x d_3 - (B_x + C_x)d_2 - F_x d_1 = 0\,. \tag{5.7}$$

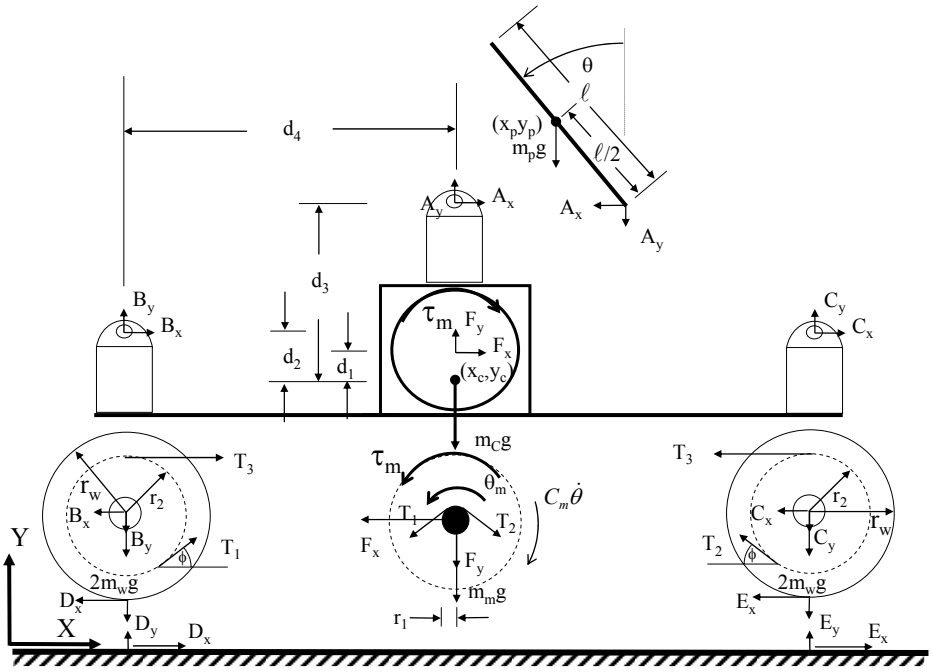

Figure 5.1: IP Cart Free Body Force Diagram

Assuming rolling without slip and that the wheels do not leave the surface, the equations for the back and front wheels are

$$T_3 + T_1\cos(\phi) - B_x - D_x = 2m_w\ddot{x}_c\,, \tag{5.8}$$

$$T_1\sin(\phi) - B_y - D_y - 2m_w g = 0\,, \tag{5.9}$$

$$-T_3 r_2 + T_1 r_2 - D_x r_w = I_w\ddot{\theta}_w\,, \tag{5.10}$$

$$-T_3 - T_2\cos(\phi) - C_x - E_x = 2m_w\ddot{x}_c\,, \tag{5.11}$$

$$T_2\sin(\phi) - C_y - E_y - 2m_w g = 0\,, \tag{5.12}$$

and

$$T_3 r_2 - T_2 r_2 - E_x r_w = I_w\ddot{\theta}_w\,. \tag{5.13}$$

The dynamic equations for the motor sprocket are

$$-F_x - T_1\cos(\phi) + T_2\cos(\phi) = m_m\ddot{x}_c\,, \tag{5.14}$$

$$-F_y - T_1 \sin(\phi) - T_2 \sin(\phi) - m_m g = 0\,, \tag{5.15}$$

and

$$\tau_m - r_1(T_1 - T_2) - C_v \dot{\theta}_m = I_m \ddot{\theta}_m\,. \tag{5.16}$$

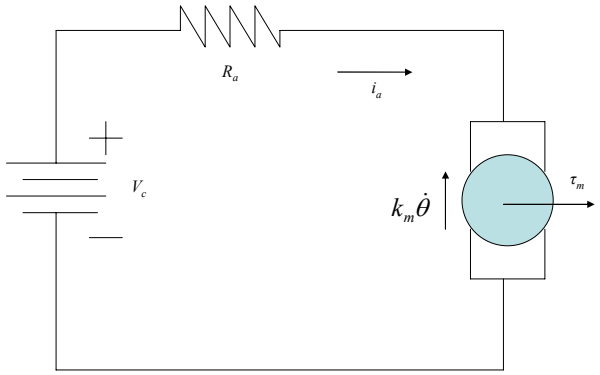

Figure 5.2: Motor Electrical Diagram

Assuming negligible armature inductance and using Figure 5.2, the electrical dynamics of the motor can be written as

$$V_c = R_a i_a + k_m \dot{\theta}_m\,, \tag{5.17}$$

and

$$\tau_m = k_t i_a\,. \tag{5.18}$$

Several kinematic equations can also be written to express the position of the center of mass of the pendulum in terms of the cart position and pendulum angle, mainly

$$x_p = x_c - \frac{l}{2}\sin(\theta), \tag{5.19}$$

and

$$y_p = y_c + \frac{l}{2}\cos(\theta) + d_3\,. \tag{5.20}$$

Differentiating equations (5.19) and (5.20) twice, with respect to time, yields,

$$\ddot{x}_p = \ddot{x}_c - \frac{l}{2}\sin(\theta)\dot{\theta}^2 - \frac{l}{2}\cos(\theta)\ddot{\theta}\,, \tag{5.21}$$

and

$$\ddot{y}_p = -\frac{l}{2}\cos(\theta)\dot{\theta}^2 - \frac{l}{2}\sin(\theta)\ddot{\theta}\,. \tag{5.22}$$

Several other kinematic relationships can be written based on the system geometry, these are

$$r_2 = 4r_1, \tag{5.23}$$

where 4=gear ratio,

$$\theta_w = -\frac{x_c}{r_w}, \dot{\theta}_w = -\frac{\dot{x}_c}{r_w}, \ddot{\theta}_w = -\frac{\ddot{x}_c}{r_w}, \tag{5.24}$$

$$\theta_m = -\frac{r_2 x_c}{r_1 r_w}, \dot{\theta}_m = -\frac{r_2 \dot{x}_c}{r_1 r_w}, \text{and} \ddot{\theta}_m = -\frac{r_2 \ddot{x}_c}{r_1 r_w}. \tag{5.25}$$

Using the dynamic equations (5.1-5.16), the electric equations (5.17,5.18), and the kinematic relationships from equations (5.19-5.25) the dynamic equations can be reduced to a two degree of freedom system written in the form of equation (2.1) as

$$\begin{bmatrix} \frac{4r_2 I_m}{r_w^2 r_1} + m_p + m_c + m_m + 4m_w + \frac{2I_w}{r_w^2} & \frac{-m_p l\cos(\theta)}{2} \\ \frac{-m_p l\cos(\theta)}{2} & \frac{m_p l^2}{3} \end{bmatrix} \begin{bmatrix} \ddot{x}_c \\ \ddot{\theta} \end{bmatrix} + \begin{bmatrix} 0 & \frac{m_p l \sin(\theta)\dot{\theta}}{2} \\ 0 & 0 \end{bmatrix} \begin{bmatrix} \dot{x}_c \\ \dot{\theta} \end{bmatrix}$$
$$+ \begin{bmatrix} \frac{4r_2\left(C_m + \frac{k_t k_m}{R_a}\right)}{r_w^2 r_1} & 0 \\ 0 & 0 \end{bmatrix} \begin{bmatrix} \dot{x}_c \\ \dot{\theta} \end{bmatrix} + \begin{bmatrix} 0 \\ -\frac{m_p g l \sin(\theta)}{2} \end{bmatrix} = \begin{bmatrix} \frac{r_2 k_t V_c}{r_w r_1 R_a} \\ 0 \end{bmatrix}. \tag{5.26}$$

The Inverted Pendulum Cart System ID

While some of the parameters in the model such as the mass of the cart/pendulum, pendulum length, and the radiuses of the wheels and sprocket are easy to obtain (Table 5.1), the viscous friction coefficient (C_m) and inertia of the drive assembly cannot be determined through direct measurement. Because of this, some form of system identification is required. To determine these unknown parameters, let us assume that the pendulum is fixed in the upright position in such a way that it cannot move (i.e. $\ddot{\theta} = \dot{\theta} = \theta = 0$), and that the cart is lifted off of the ground so that the translational inertia does not contribute to the dynamic response. These assumptions result in the following second order differential equation

$$A_2 \ddot{x}_c + A_3 \dot{x}_c = A_4 V_c, \tag{5.27}$$

with a solution of

$$\dot{x}_c = \frac{A_4}{A_3}\left(1 - e^{\frac{A_3}{A_2}(t-t_0)}\right) V_c, \tag{5.28}$$

where

$$A_2 = \frac{4r_2 I_m}{r_w^2 r_1} + \frac{2I_w}{r_w^2}, \tag{5.29}$$

$$A_3 = \frac{4r_2\left(C_m + \frac{k_t k_m}{R_a}\right)}{r_w^2 r_1}, \tag{5.30}$$

$$A_4 = \frac{r_2 k_t}{r_w r_1 R_a}. \tag{5.31}$$

By setting the cart up on blocks and applying step inputs to the motor and measuring the response we can determine the unknown parameters A_2 and A_3. A_4 was determined through measuring the various components and consulting the motor manufacturers' documentation.

A 6024E National Instruments (NI) DAQCard was used to provide a step voltage in conjunction with NI LabVIEW 8.2 and a quadrature encoder to measure the cart position. A finite difference technique was then applied to estimate the cart "velocity". The identification of A_2 and A_3 was done in two stages. First the data from when the cart had reached a steady state velocity (i.e. $\ddot{x}_c = 0$) was used to determine A_3 using equation (5.27). Then least sum squares was used to minimize the error between the estimated velocity from the measured data and equation (5.28) utilizing Microsoft Excel solver. This technique was done for step voltages of 3, 6, 9 and 12 volts and the results were then averaged. Figure 5.3 shows an example of the curve fitting solution. Table 5.1 contains the results of the system identification and the rest of the parameter values.

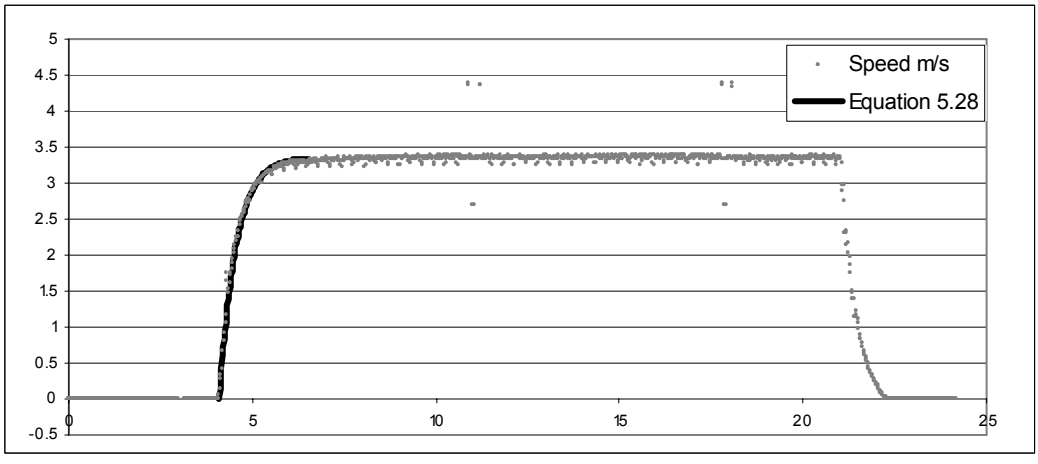

Figure 5.3: ID Data for 3 Volts

Table 5.1: IP Cart System Identification

Quantity	Value	Quantity	Value
$m_p + m_c + m_m + 4m_w$	10.1206 *Kg*	R_a	3.14398 Ω
K_t	.100142 *Nm/amp*	l	.8509 *m*
K_m	.100142 *Vs/rad*	R_w	.0631*m*
g	9.80093 m/s^2	r_2/r_1	4
A_2	1.964283 *Kg*	A_3	6.4777 *Ns/m*
A_4	1.859456 *N/V*	*Amp Gain*	3

Figure 5.4: Inverted Pendulum Cart

The Inverted Pendulum Cart Hard Real-time Implementation

A controller based upon the direct Lyapunov approach, as outlined in Chapter 2, was formulated. The control law was then implemented in hard real time on a PC running LabVIEW Real Time 8.2.1 using 1st order Euler integration and a sample rate of 400 Hz. Once again, a 6024E National Instruments (NI) DAQCard was used for data acquisition and control signal output. A Lambda F28-M power supply set to 30 volts and an Advanced Motion Control 25A8K voltage amplifier with a gain of 3 was used to increase the implementable control signal range. To accommodate the amp gain, A_4 was multiplied by three, allowing for the control law to be expressed in terms of DAQ voltage. Using the system identification presented in Table 5.1, a linear observer was designed to estimate the cart and pendulum velocities (Chen 1998). A linear observer should be sufficiently accurate provided that the displacement of the pendulum remains small. The DLA controller parameters and observer poles are found in Table 5.2. The LabVIEW VIs are found in Appendix 1.

Table 5.2: DLA Implementation Parameters

Quantity	Value	Quantity	Value
Obs. Poles	-10,-11,-12,-13	β	-100.0
a_1	.2 *m*	ω	0.25 *rad/s*
γ	0. 5	α	1.0
$\boldsymbol{K}_{Df}$	$\begin{bmatrix} 40.0 & -50.0 \\ -50.0 & 75.0 \end{bmatrix}$	$\boldsymbol{\Lambda}$	$\begin{bmatrix} 0.85 & 0.0 \\ 0.0 & 1.7 \end{bmatrix}$

As in Chapter 3, the last row of (2.2) was used to determine a differential equation for the desired pendulum angle and the control law component $\boldsymbol{u}_2$ was chosen to provide stabilization to this equation as

$$\begin{aligned} \boldsymbol{u}_2 \equiv & \frac{1}{2} m_p l \cos(\theta)\left(\ddot{x}_d - \lambda_1\left(\dot{x} - \dot{x}_d\right)\right) + \frac{1}{2} m_p l \sin(\theta) \\ & \frac{1}{2}\gamma m_p l \cos(\theta)\left(\dot{x} - \dot{x}_d + \lambda_1\left(x - x_d\right)\right) + \frac{1}{3} m_p l^2 \left(\gamma\left(\dot{\theta} - \dot{\theta}_d\right) + \lambda_2 \dot{\theta}\right) \end{aligned} . \tag{5.32}$$

The control law component $\boldsymbol{u}_1$ was chosen as (2.35). A desired trajectory was defined for the cart as $x_d = a_1(1-\cos(\omega t))$ with a_1 and ω as defined in Table 5.2. The matrix $\boldsymbol{K}_{Df}$ was chosen to be

positive definite and symmetric and the matrix $\boldsymbol{A}$ was chosen with the intention of placing greater relative weighting on the cart position. The system was operated for a period of 60 seconds and the measurements were communicated back to a PC running LabVIEW 8.2. Figures 5.5 and 5.6 contain the desired and measured trajectories during the system maneuver.

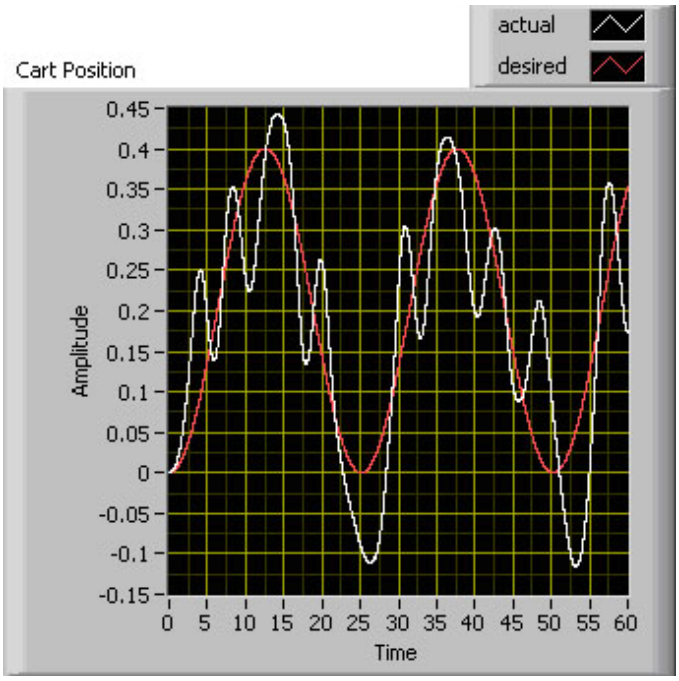

Figure 5.5: Cart Position

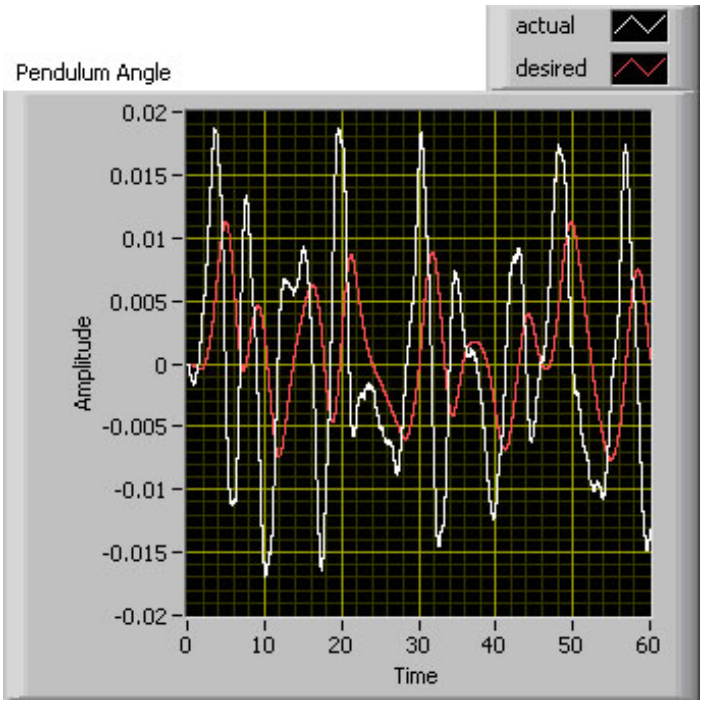

Figure 5.6: Pendulum Position

Upon examining Figures 5.5 and 5.6 we see that the cart tends to track the desired path but the performance is not very good. There are several possibilities that may account for the poor tracking performance. The largest single factor that negatively affects the performance is probably the lack of static friction in the developed dynamic model. Since the velocity of the cart remains small, static friction plays a significant role in the dynamics response. An antisticktion sub VI was implemented to help offset the influence of static friction; however, it is thought that it would be beneficial to include a model of the static friction in the controller development. Alternatively, increasing the amplitude for the desired cart trajectory may help to limit the effect of static friction on the system. Unfortunately the power cord and encoder cables were a limiting factor on the size of this parameter.

The relatively low sample rate of 400 Hz is also thought to be a factor in the poor performance. Past experience, with linear feedback controllers, has shown that a sample rate of 5000 Hz is desired for real time implementations on with this system. The sample rate was dictated by the high overhead associated with using a function node for the DLA controller calculation within LabVIEW Real Time 8.2.1. Optimization of the VI or a new version of LabVIEW may increase the available sample rate. Lastly, from experience with the simulated models presented in Chapters 3 and 4, tuning of the controller constants can play a substantial role in improving the tracking performance. Unfortunately time constraints prevented the tuning of these parameters to improve the tracking performance of the presented system. To date there are no guidelines for the tuning of these parameters and this is an opportunity for future research.

Chapter Summary

In this chapter, the laboratory inverted pendulum cart system has been presented. A dynamic model was developed and system identification was performed to determine certain parameters. The DLA control strategy was implemented in hard real time using LabVIEW 8.2. The DLA controller did not perform as well as expected. Several reasons, such as unmodeled static friction and poor constant selection, etc., have been identified for the poor performance and possible solutions outlined.

CHAPTER 6 - Conclusions and Recommendations

In this thesis a novel feedback control scheme for trajectory tracking of underactuated mechanical systems was developed using the direct Lyapunov approach. A literary survey is given in Chapter 1 along with a discussion of control approaches of underactuated mechanical systems, specifically their features and limitations. The scalability limitations of the current control techniques and observed undesirable performance characteristics are the main motivations of this work.

In Chapter 2, the formulation of the proposed control techniques is presented in detail. The candidate Lyapunov function, $V(\boldsymbol{s},t)$ is defined with $\boldsymbol{K}_D$ used to represent the kinetic and potential part of the candidate Lyapunov function. The sliding mode control law presented in Slotine and Li (1988) in which the lower *n-m* equations are zero due to the underactuation of the control input vector provides a basis for the control law. Three matching equations are developed from the derivative of the candidate Lyapunov function. These matching equation are used to determine the matrices $\boldsymbol{K}_D$ and $\boldsymbol{K}_v$, and the tracking control law. There are two remarkable results of the tracking controller development. The first is that we arrived at three matching equations that are (with the exception of $\overline{\boldsymbol{K}}_D$) identical to matching equations developed for stabilization as shown in White et al. (2006, 2007, 2008). The second is that it is not necessary to perform inverse dynamics for specifying every coordinate history for the control law implementation. Instead, the control law provides a means for determining the necessary unspecified coordinate histories.

A discussion on following a path and a solution strategy is presented for determining the positive definite function $\Psi(\boldsymbol{s},\boldsymbol{u})$. This strategy does not guarantee the positive definiteness of $\Psi(\boldsymbol{s},\boldsymbol{u})$ when $\|\boldsymbol{s}\|$ becomes small. As a result the tracking error variable ($\boldsymbol{s}$) is not asymptotically stabilized. The $\|\boldsymbol{s}\|$ is instead reduced to within an ultimate bound. Lemma 2.1 provides a means for the estimation of this ultimate bound based upon the matrices $\boldsymbol{K}_D$ and $\boldsymbol{K}_v$ and the vector $\boldsymbol{u}$.

In Chapter 3, two holonomic applications are presented to illustrate the versatility and performance of the proposed control technique. The inverted pendulum cart was presented as the first example. In this example a desired trajectory was tracked by the cart, or the actuated

axis, and the control law was used to determine a desired trajectory for the pendulum, or unactuated axis. Alternatively, in the second example, the ball and beam, a desired trajectory was specified for the ball, or unactuated axis, and the control law was used to determine the desired system trajectory for the beam, or actuated axis. In addition, an example of stabilization in the tracking sense was done for the inverted pendulum cart. This example was shown to be robust to identification errors and disturbances.

Chapter 4 presented an example of a nonholonomic system, the rolling wheel. Three control schemes were presented for this system. The first was a feedforward scheme in which inverse dynamics were used to determine the desired system trajectories and control torques required for the wheel to roll in a figure eight shaped path in the X-Y plane. In the second, the direct Lyapunov approach was used along with the desired system trajectories determined in the feedforward example. The third example used the direct Lyapunov approach but differed in that it used the control law, and not the system dynamic equations alone, to determine the desired history of the wheel tilt angle. Both of the direct Lyapunov approach examples were shown to be robust to step disturbances and initial condition errors.

Chapter 5 presented an implementation of the DLA control strategy on a holonomic system, the inverted pendulum cart. A dynamic model was developed and system identification was performed to determine certain parameters in the model. Next, the control law was implemented using LabVIEW Real Time 8.2.1 with a sample rate of 400 Hz. From the plots of the hard real time data, the tracking performance of the controller was shown to be somewhat poor. Some possible reasons for the poor performance include, low sample rate, unmodeled static friction, and poor controller parameter selection. Addressing all, or a subset, of these issues should lead to better tracking performance.

In order to increase the usefulness and acceptance of the direct Lyapunov approach as a viable and useful control scheme, some recommendations are provided. These are:

- Several modifications should be made to the laboratory inverted pendulum cart system to insure that a uniform, repeatable, system response can be obtained. Then the control algorithm for the hard real time implementation should be tuned by adjusting the various parameters in the control law to determine if a better response at a 400 Hz sample rate is achievable.

- Research into possible techniques for determining $\Psi(\boldsymbol{s},\boldsymbol{u})$ such that is remains a positive definite function should be carried out.

- If $\Psi(\boldsymbol{s},\boldsymbol{u})$ can not be made to be positive definite, additional research should be done to increase the accuracy of estimating the ultimate bound.

- Develop tools to aid in choosing controller parameters and constants.

- Can the matrix $\boldsymbol{K}_D$ be made a function of $\boldsymbol{q}$ alone?

- The control algorithm should be tested on a real rolling wheel system such as presented in Xu et al. (2004) to validate the simulation results and provide a useful guide for expected controller performance.

References

Acosta, J. A., R. Ortega, A. Astolfi and A. D. Mahindrakar (2005). Interconnection and damping assignment passivity–based control of mechanical systems with underactuation degree one. *IEEE Trans. Automatic Control,* 50(12), 1936-1955.

Ashrafiuon, Hashem, R., Scott Erwin (2004). Sliding Control Approach to Underactuated Multibody Systems. *Proceeding of the American Control Conference*, Boston, Massachusetts (pp.1283 – 1288).

Auckly, D, L. Kapitanski, and W. White (2000). Control of Nonlinear Underactuated Systems. *Comm. Pure Appl. Math*, 53(3), 354-369.

Blajer, Wojciecj and Krzysztof Kolodziejczyk (2007). Control of Underactuated Mechanical Systems with Servo-Constraints. *Nonlinear Dynamics***,** 50(4), 781 – 791.

Bloch, Anthony M., Naomi Ehrich Leonard, and Jerrold E. Marsden (2000). Controlled Lagrangians and the Stabilization of Mechanical Systems. I: The First Matching Theorem. *IEEE Transactions on Automatic Control*, 45(12), 2253-2270.

Bloch, A.M., Dong Eui Chang, N.E. Leonard, J.E. Marsden (2001). Controlled Lagrangians and the stabilization of mechanical systems. II. Potential Shaping. *IEEE Transactions on Automatic Control*, 46(10), 1556 – 1571

Bošković, Dejan M., and Miroslav Krstić (1999). Global attitude/position regulation for underwater vehicles. *International Journal of Systems Science*, 30(9), 939-946.

Chen, Chi-Tsong (1998). *Linear System Theory and Design*. NY: Oxford University Press, 1998

Do, K. D., Z. P. Jiang and J. Pan (2002). Underactuated ship global tracking under relaxed conditions. *IEEE Transactions on Automatic Control*, 47(9), 1529-1536, 2002.

Driessen, Brian J. and Nader Sadegh (2000). Minimum-Time Trajectory Tracking of an Under-Actuated System. *Proceedings of the American Control Conference*, Chicago, Illinois (pp. 2834 – 2838).

Gomez-Estern, F., A.J. Van der Schaft, and J.A. Acosta (2004). Passivation of underactuated systems with physical damping. *6th IFAC Symposium on Nonlinear Control Systems (NOLCOS 2004)*, 3(3), 1235-40.

Greenwood, Donald T. (2003). *Advanced Dynamics*. Cambridge UK: Cambridge Univ. Press.

Hongrui, Wang, Tian Yantao, Fu Siyan, and Sui Zhen (2008). Nonlinear Control for Output Regulation of Ball and Plate System. *Proceedings of the 27th Chinese Control Conference*, Kunming, Yunnan (pp. 382-387).

Jain, Abhinandan and Guillermo Rodriguez (1991). An Analysis of the Kinematics and Dynamics of Underactuated Manipulators. *IEEE Transactions on Robots and Automation*, 9(4), 411 – 422.

Khalil, Hassan K. (2002). *Nonlinear Systems*. Upper Saddle River, NJ: Prentice-Hall.

Laila, Dina Shona and Alessandro Astolfi (2006). Discrete-time IDA-PBC design for underactuated Hamiltonian control systems. *Proceedings of the American Control Conference*, Minneapolis, Minnesota (pp. 188-193).

NLCLab.mne.ksu.edu (2007). <http://www.mne.ksu.edu/research/laboratories/non-linear-controls-lab/non-linear-home>.

Olfati-Saber, Reza and Alexandre Megretski (1998). Control for a Class of Underactuated Nonlinear Systems. *Proceedings of the IEEE Conference on Decision and Control*, 4182-4187.

Olfati-Saber, Reza (2000). Control of Underactuated Mechanical Systems with Two Degrees of Freedom and Symmetry. *Proceedings of the American Control Conference*, Chicago, Illinois (pp. 4092-4096).

Olfati-Saber, Reza (2001). *Nonlinear Control of Underactuated Systems with Application to Robotics and Aerospace Vehicles*. Doctoral disertation, Massachusetts Institute of Technology, Department of Electrical and Computer Science.

Ortega, Romeo, Mark W. Spong, Fabio Gómez-Estern, and Guido Blankenstein (2002). Stabilization of a Class of Underactuated Mechanical Systems Via Interconnection and Damping Assignment. *IEEE Transactions on Automatic Control*, 47(8), 1218-1233.

Rosas-Flors, J. Alfredo, Jaime Alvarez-Gallegos, and Rafael Castro-Linares (2001). Trajectory Planning and Control of an Underactuated Planar 2R Manipulator. *Proceeding of the IEEE International Conference on Control Applications*, Mexico City, Mexico pp. 548-552.

Sandoz, Eric E., Peter V. Kokotović, and João P. Hespanha (2008). Trackablility Filtering for Underactuated Systems. *Proceeding of the American Control Conference*, Seattle, Washington (pp. 1758-1763).

Singhal, Rakesh, Rupesh Patayane, and Ravi N. Banavar (2006). Tracking a Trajectory for a Gantry Crane: Comparison Between IDA-PBC and Direct Lyapunov Approach. *IEEE International Conference on Industrial Technology*, 1788-1793.

Slotine, Jean-Jacques E. and Weiping Li (1998). Adaptive Manipulator Control: A Case Study. *IEEE Transactions on Automatic Control*, 33(11), 995-1003.

Wang, Z., P. Goldsmith (2008). Modified energy-balancing-based control for the tracking problem. *The Institute of Engineering and Technology Control Theory and Applications.* 2(4), 310-312.

White, Warren N., Mikil Foss, and Xin Guo (2006). A Direct Lyapunov Approach for a Class of Underactuated Mechanical Systems. *Proceedings of the American Control Conference*, Minneapolis, Minnesota (pp. 103-110).

White, Warren N., Mikil Foss, and Xin Guo (2007). A Direct Lyapunov Approach for Stabilization of Underactuated Mechanical Systems. *Proceedings of the American Control Conference*, New York, NY (pp. 4817-4822).

White, Warren N., Mikil Foss, Jaspen Patenaude, Xin Guo, and Deyka Garcia (2008). Improvements in Direct Lyapunov Stabilization of Underactuated, Mechanical Systems. *Proceedings of the American Control Conference*, Seattle, WA (pp. 2927-2932).

Xu, Yangsheng and Samuel Kwok-Wai Au (2004). Stabilization and Path Following of a Single Wheel Robot. *IEEE Transactions on Mechatronics*, 9, 407-419.

Appendix A - LabVIEW VIs

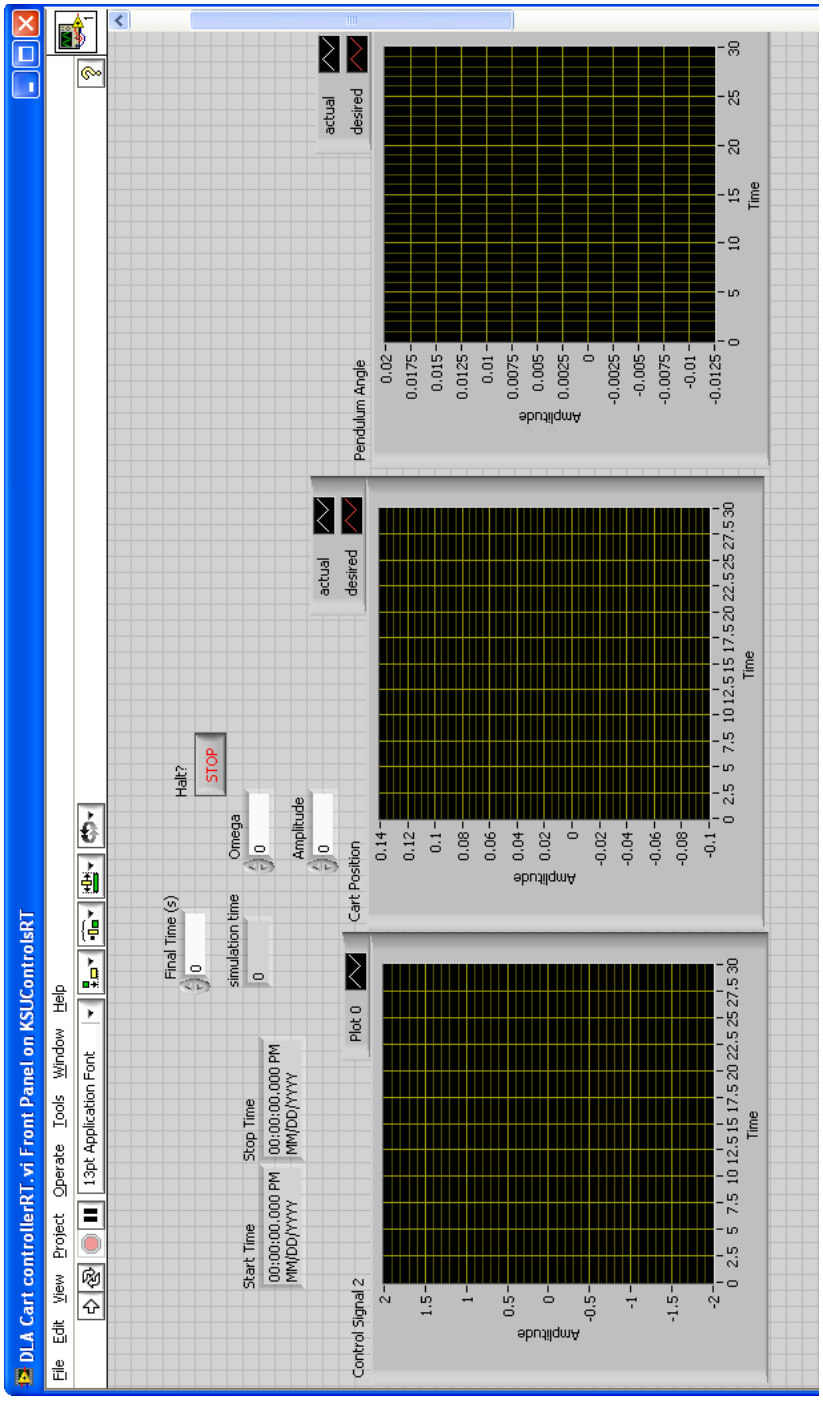

DLA Real Time Implementation-Front Panel

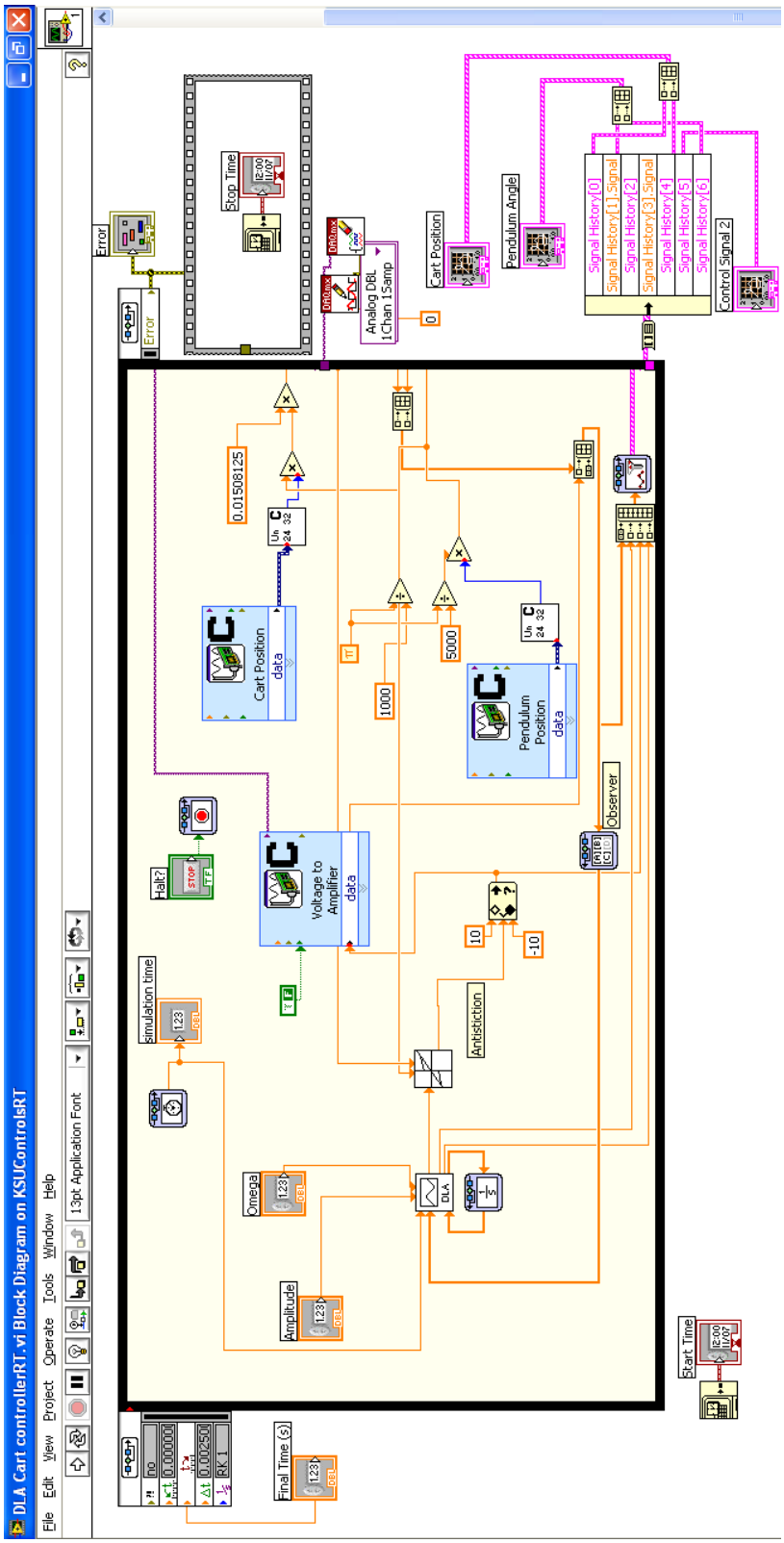

DLA Real Time Implementation-Block Diagram

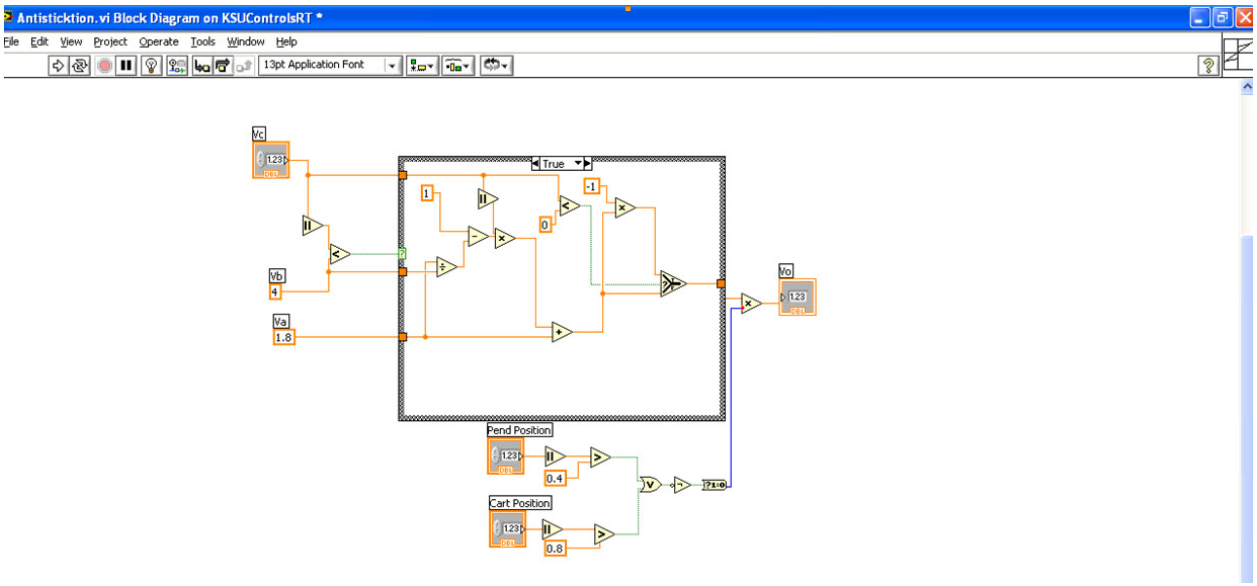

Antisticktion sub .vi-Block Diagram

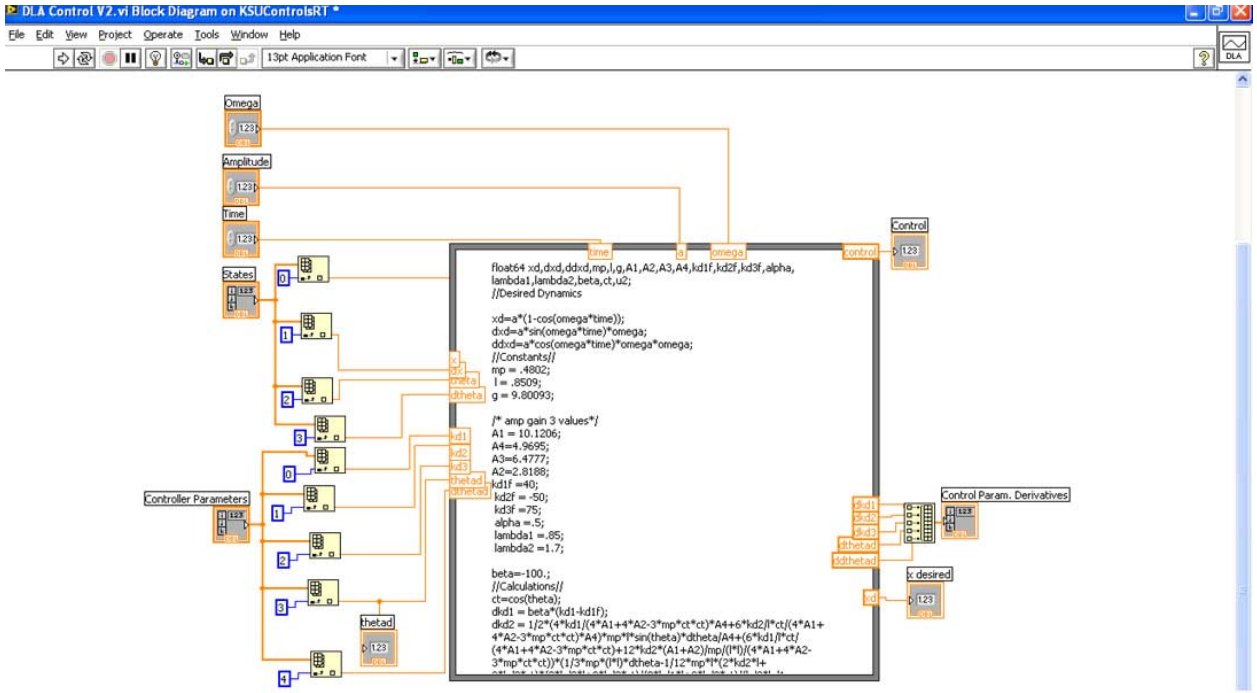

DLA sub .vi-Block Diagram

DLA sub .vi Code

```
//Declare variables
float64 xd,dxd,ddxd,mp,l,g,A1,A2,A3,A4,kd1f,kd2f,kd3f,alpha,lambda1,lambda2,beta,ct,u2;

//Desired Dynamics
xd=a*(1-cos(omega*time));// desired x position (m)
dxd=a*sin(omega*time)*omega;// desired x velocity(m/s)
ddxd=a*cos(omega*time)*omega*omega;// desired x acceleration (m/s^2)

//System ID
mp = .4802; //Pendulum Mass Kg
 l = .8509; //Pendulum Length m
g = 9.80093; //Local acceleration of gravity
A1 = 10.1206;
A4=4.9695;
A3=6.4777;
A2=2.8188;

// Control Constants
kd1f =40.;
kd2f = -50.;
kd3f =75.;
alpha =.5;
lambda1 =.85;
lambda2 =1.7;
beta=-100.;

//     d(KD)/dt Calculations
ct=cos(theta);
dkd1 = beta*(kd1-kd1f);
dkd2 = 1/2*(4*kd1/(4*A1+4*A2-3*mp*ct*ct)*A4+6*kd2/l*ct/(4*A1+4*A2-
3*mp*ct*ct)*A4)*mp*l*sin(theta)*dtheta/A4+(6*kd1/l*ct/(4*A1+4*A2-
3*mp*ct*ct)+12*kd2*(A1+A2)/mp/(l*l)/(4*A1+4*A2-3*mp*ct*ct))*(1/3*mp*(l*l)*dtheta-
1/12*mp*l*(2*kd2*l+3*kd3*ct)*(2*kd2*l+3*kd3*ct)/(2*kd1*l+3*kd2*ct)/(kd3*kd1-kd2*kd2)*beta*(kd1-
kd1f)+1/6*(2*kd2*l+3*kd3*ct)*mp*l/(kd3*kd1-kd2*kd2)*beta*(kd2-kd2f)-
1/12*(2*kd1*l+3*kd2*ct)*mp*l/(kd3*kd1-kd2*kd2)*beta*(kd3-kd3f))+beta*(kd2-kd2f);
dkd3 = (4*kd2/(4*A1+4*A2-3*mp*ct*ct)*A4+6*kd3/l*ct/(4*A1+4*A2-
3*mp*ct*ct)*A4)*mp*l*sin(theta)*dtheta/A4+2*(6*kd2/l*ct/(4*A1+4*A2-
3*mp*ct*ct)+12*kd3*(A1+A2)/mp/(l*l)/(4*A1+4*A2-3*mp*ct*ct))*(1/3*mp*(l*l)*dtheta-
1/12*mp*l*(2*kd2*l+3*kd3*ct)*(2*kd2*l+3*kd3*ct)/(2*kd1*l+3*kd2*ct)/(kd3*kd1-kd2*kd2)*beta*(kd1-
kd1f)+1/6*(2*kd2*l+3*kd3*ct)*mp*l/(kd3*kd1-kd2*kd2)*beta*(kd2-kd2f)-
1/12*(2*kd1*l+3*kd2*ct)*mp*l/(kd3*kd1-kd2*kd2)*beta*(kd3-kd3f))+beta*(kd3-kd3f);

//Linear DLA Control law-used for testing purposes
/*control=(10.5502)*x+(15.7776)*dx+(-100.3822)*theta+(-31.3320)*dtheta;*/

//                          U calc-chosen by feedback linearization to stabilize ddthetad equation
u2 = 1/2*mp*l*ct*(ddxd-lambda1*(dx-dxd))+1/2*mp*g*l*sin(theta)-1/2*alpha*mp*l*ct*(dx-dxd+lambda1*(x-
xd))+1/3*alpha*mp*l*l*(dtheta-dthetad)+1/3*lambda2*mp*l*l*dtheta;

//                      theta desired calculation-integrated wrt
ddthetad =3*(1/2*mp*l*ct*(ddxd-lambda1*(dx-dxd))-1/3*mp*l*l*dtheta*(dthetad-lambda2*(theta-
thetad))+1/2*mp*g*l*sin(theta)-u2-1/2*alpha*mp*l*ct*(dx-dxd+lambda1*(x-xd))+1/3*alpha*mp*l*l*(dtheta-
dthetad+lambda2*(theta-thetad)))/mp/(l*l)+lambda2*(dtheta-dthetad);
```

```
//                Control Law Caclulation
control=(A1+A2)/A4*(ddxd-lambda1*(dx-dxd))-1/2*mp*l*ct/A4*(ddthetad-lambda2*(dtheta-
dthetad))+A3/A4*(dxd-lambda1*(x-xd))+1/2*mp*l*sin(theta)*dtheta/A4*(dthetad-lambda2*(theta-
thetad))+1/2/A4*(-
18*kd3*kd3*A2*ct*g*sin(theta)+18*kd3*kd3*A2*ct*ct*alpha*dx+18*kd3*kd3*A2*ct*ct*alpha*lambda1*x-
12*kd3*kd3*A2*ct*alpha*l*dtheta-12*kd3*kd3*A2*ct*lambda2*l*dtheta+6*dx*kd1*l*l*mp*ct*ct-
12*l*dx*kd2*ct*A1-12*l*dx*kd2*ct*A2+9*l*dx*kd2*ct*ct*ct*mp+6*dtheta*kd2*l*l*mp*ct*ct-
12*l*dtheta*kd3*ct*A1-12*l*dtheta*kd3*ct*A2+9*l*dtheta*kd3*ct*ct*ct*mp-8*lambda2*theta*kd2*l*l*A1-
8*lambda2*theta*kd2*l*l*A2-12*kd3*A2*kd2*l*ct*ddxd-12*kd3*A1*kd2*l*alpha*ct*dxd-
12*kd3*A1*kd2*l*alpha*ct*lambda1*xd-12*kd2*A2*kd1*l*alpha*ct*dxd-
12*kd2*A2*kd1*l*alpha*ct*lambda1*xd-18*kd2*kd2*A2*ct*ct*lambda1*dxd-18*kd2*kd2*A2*ct*ct*alpha*dxd-
6*kd2*kd2*ct*ct*mp*l*l*ddxd-9*kd1*ct*ct*ct*mp*l*kd2*ddxd-9*kd1*ct*ct*ct*mp*l*kd2*lambda1*dxd-
9*kd1*ct*ct*ct*mp*l*kd2*alpha*dxd-9*kd1*ct*ct*ct*mp*l*kd2*alpha*lambda1*xd-
18*kd2*kd2*A2*ct*ct*alpha*lambda1*xd+12*kd2*kd2*A2*ct*alpha*l*dthetad+12*l*lambda1*xd*kd2*ct*A2-
9*l*lambda1*xd*kd2*ct*ct*ct*mp-
6*kd2*kd2*ct*ct*mp*l*l*lambda1*dxd+6*kd1*ct*ct*mp*l*l*kd2*alpha*dthetad-12*kd2*A1*kd1*l*ct*ddxd-
12*kd2*A1*kd1*l*ct*lambda1*dxd-
6*lambda1*xd*kd1*l*l*mp*ct*ct+8*kd2*A1*kd1*l*l*alpha*dthetad+12*l*lambda1*xd*kd2*ct*A1-
12*kd2*A1*kd1*l*alpha*ct*dxd-12*kd2*A1*kd1*l*alpha*ct*lambda1*xd-
18*kd2*kd2*A1*ct*ct*alpha*dxd+8*kd2*A2*kd1*l*l*alpha*dthetad-12*kd3*A2*kd2*l*ct*lambda1*dxd-
12*kd3*A2*kd2*l*alpha*ct*dxd-12*kd3*A2*kd2*l*alpha*ct*lambda1*xd-18*kd3*kd3*A2*ct*ct*lambda1*dxd-
9*kd2*ct*ct*ct*mp*l*kd3*alpha*dxd-
9*kd2*ct*ct*ct*mp*l*kd3*alpha*lambda1*xd+6*kd2*ct*ct*mp*l*l*kd3*alpha*dthetad-
6*kd2*kd2*ct*ct*mp*l*l*alpha*dxd-
6*kd2*kd2*ct*ct*mp*l*l*alpha*lambda1*xd+4*kd2*kd2*ct*mp*l*l*l*alpha*dthetad-8*lambda1*x*kd1*l*l*A1-
8*lambda1*x*kd1*l*l*A2-12*kd3*kd3*A1*ct*lambda2*l*dtheta-
12*kd3*A1*kd2*l*g*sin(theta)+12*kd3*A1*kd2*l*alpha*ct*dx+12*kd3*A1*kd2*l*alpha*ct*lambda1*x+18*kd3
*kd3*A1*ct*ct*lambda1*dx+12*kd2*A2*kd1*l*alpha*ct*lambda1*x+18*kd2*kd2*A2*ct*ct*lambda1*dx-
18*kd2*kd2*A2*ct*g*sin(theta)+18*kd2*kd2*A2*ct*ct*alpha*dx+18*kd2*kd2*A2*ct*ct*alpha*lambda1*x+9*k
d1*ct*ct*ct*mp*l*kd2*lambda1*dx-
9*kd1*ct*ct*mp*l*kd2*g*sin(theta)+9*kd1*ct*ct*ct*mp*l*kd2*alpha*dx+9*kd1*ct*ct*ct*mp*l*kd2*alpha*lamb
da1*x+8*dthetad*kd2*l*l*A1-12*kd2*kd2*A2*ct*alpha*l*dtheta-
12*kd2*kd2*A2*ct*lambda2*l*dtheta+6*kd2*kd2*ct*ct*mp*l*l*lambda1*dx-
6*kd2*kd2*ct*mp*l*l*g*sin(theta)+6*kd2*kd2*ct*ct*mp*l*l*alpha*lambda1*x-
6*kd1*ct*ct*mp*l*l*kd2*alpha*dtheta-
6*kd1*ct*ct*mp*l*l*kd2*lambda2*dtheta+12*kd2*A1*kd1*l*ct*lambda1*dx-
12*kd2*A1*kd1*l*g*sin(theta)+12*kd2*A1*kd1*l*alpha*ct*dx+8*dthetad*kd2*l*l*A2-
8*kd2*A1*kd1*l*l*alpha*dtheta-8*kd2*A1*kd1*l*l*lambda2*dtheta-
18*kd3*kd3*A2*ct*ct*ddxd+12*kd2*A1*kd1*l*alpha*ct*lambda1*x+18*kd2*kd2*A1*ct*ct*lambda1*dx-
18*kd2*kd2*A1*ct*g*sin(theta)+18*kd2*kd2*A1*ct*ct*alpha*dx+18*kd2*kd2*A1*ct*ct*alpha*lambda1*x-
8*kd2*A2*kd1*l*l*alpha*dtheta-9*kd2*ct*ct*ct*mp*l*kd3*ddxd-
9*kd2*ct*ct*ct*mp*l*kd3*lambda1*dxd+8*kd3*A1*kd2*l*l*alpha*dthetad-
6*lambda2*thetad*kd2*l*l*mp*ct*ct+12*l*lambda2*thetad*kd3*ct*A1+12*l*lambda2*thetad*kd3*ct*A2-
9*l*lambda2*thetad*kd3*ct*ct*ct*mp-6*kd1*kd1*ct*ct*mp*l*l*ddxd+12*l*dthetad*kd3*ct*A2-
12*kd3*A1*kd2*l*ct*ddxd-12*kd3*A1*kd2*l*ct*lambda1*dxd-18*kd3*kd3*A1*ct*ct*lambda1*dxd-
18*kd3*kd3*A1*ct*ct*alpha*dxd-18*kd3*kd3*A1*ct*ct*alpha*lambda1*xd+8*kd3*A2*kd2*l*l*alpha*dthetad-
9*l*dthetad*kd3*ct*ct*ct*mp+12*l*dxd*kd2*ct*A2-9*l*dxd*kd2*ct*ct*ct*mp-
18*kd2*kd2*A1*ct*ct*alpha*lambda1*xd+12*kd2*kd2*A1*ct*alpha*l*dthetad-12*kd2*A2*kd1*l*ct*ddxd-
12*kd2*A2*kd1*l*ct*lambda1*dxd-6*kd1*kd1*ct*ct*mp*l*l*lambda1*dxd-
6*kd1*kd1*ct*ct*mp*l*l*alpha*dxd-
6*kd1*kd1*ct*ct*mp*l*l*alpha*lambda1*xd+4*kd1*kd1*ct*mp*l*l*l*alpha*dthetad-
18*kd2*kd2*A1*ct*ct*lambda1*dxd-
8*kd2*A2*kd1*l*l*lambda2*dtheta+8*dxd*kd1*l*l*A1+12*kd3*A2*kd2*l*ct*lambda1*dx-
12*kd3*A2*kd2*l*g*sin(theta)+12*kd3*A2*kd2*l*alpha*ct*dx+12*kd3*A2*kd2*l*alpha*ct*lambda1*x+18*kd3
*kd3*A2*ct*ct*lambda1*dx-
```

9*kd2*ct*ct*mp*l*kd3*g*sin(theta)+9*kd2*ct*ct*ct*mp*l*kd3*alpha*dx+9*kd2*ct*ct*ct*mp*l*kd3*alpha*lamb
da1*x-6*kd2*ct*ct*mp*l*l*kd3*alpha*dtheta-6*kd2*ct*ct*mp*l*l*kd3*lambda2*dtheta-
8*dtheta*kd2*l*l*A1+6*kd2*kd2*ct*ct*mp*l*l*alpha*dx-4*kd2*kd2*ct*mp*l*l*l*alpha*dtheta-
4*kd2*kd2*ct*mp*l*l*l*lambda2*dtheta+9*kd2*ct*ct*ct*mp*l*kd3*lambda1*dx-
18*kd3*kd3*A2*ct*ct*alpha*dxd-
18*kd3*kd3*A2*ct*ct*alpha*lambda1*xd+12*kd3*kd3*A2*ct*alpha*l*dthetad-
6*dxd*kd1*l*l*mp*ct*ct+12*l*dxd*kd2*ct*A1-
6*dthetad*kd2*l*l*mp*ct*ct+12*l*dthetad*kd3*ct*A1+8*lambda2*thetad*kd2*l*l*A1+8*lambda2*thetad*kd2*l
*l*A2+8*lambda1*xd*kd1*l*l*A1+8*lambda1*xd*kd1*l*l*A2+12*kd3*kd3*A1*ct*alpha*l*dthetad-
18*kd2*kd2*A2*ct*ct*ddxd-18*kd2*kd2*A1*ct*ct*ddxd-8*kd3*A1*kd2*l*l*alpha*dtheta-
8*kd3*A1*kd2*l*l*lambda2*dtheta-
12*l*lambda2*theta*kd3*ct*A2+9*l*lambda2*theta*kd3*ct*ct*ct*mp+8*dxd*kd1*l*l*A2-
8*dx*kd1*l*l*A1+12*kd3*A1*kd2*l*ct*lambda1*dx-
18*kd3*kd3*A1*ct*g*sin(theta)+18*kd3*kd3*A1*ct*ct*alpha*dx+18*kd3*kd3*A1*ct*ct*alpha*lambda1*x-
12*kd3*kd3*A1*ct*alpha*l*dtheta-8*kd3*A2*kd2*l*l*alpha*dtheta-8*kd3*A2*kd2*l*l*lambda2*dtheta-
8*dx*kd1*l*l*A2+6*kd1*kd1*ct*ct*mp*l*l*alpha*lambda1*x+6*lambda2*theta*kd2*l*l*mp*ct*ct-
12*l*lambda2*theta*kd3*ct*A1+6*lambda1*x*kd1*l*l*mp*ct*ct-12*l*lambda1*x*kd2*ct*A1-
12*l*lambda1*x*kd2*ct*A2+9*l*lambda1*x*kd2*ct*ct*ct*mp-8*dtheta*kd2*l*l*A2-
12*kd2*kd2*A1*ct*alpha*l*dtheta-12*kd2*kd2*A1*ct*lambda2*l*dtheta+12*kd2*A2*kd1*l*ct*lambda1*dx-
12*kd2*A2*kd1*l*g*sin(theta)+12*kd2*A2*kd1*l*alpha*ct*dx+6*kd1*kd1*ct*ct*mp*l*l*lambda1*dx-
6*kd1*kd1*ct*mp*l*l*g*sin(theta)+6*kd1*kd1*ct*ct*mp*l*l*alpha*dx-4*kd1*kd1*ct*mp*l*l*l*alpha*dtheta-
4*kd1*kd1*ct*mp*l*l*l*lambda2*dtheta-
18*kd3*kd3*A1*ct*ct*ddxd)/(4*kd1*kd1*l*l+12*kd1*l*kd2*ct+9*kd2*kd2*ct*ct+4*kd2*kd2*l*l+12*kd2*l*kd3
*ct+9*kd3*kd3*ct*ct)-alpha*(A1+A2)/A4*(dx-dxd+lambda1*(x-xd))+1/2*alpha*mp*l*ct/A4*(dtheta-
dthetad+lambda2*(theta-thetad))+(-1/4/A4*l*(4*A1+4*A2-3*mp*ct*ct)/(2*kd1*l+3*kd2*ct)*beta*(kd1-kd1f)-
2*A4*(2*kd1*l+3*kd2*ct)/l/(4*A1+4*A2-3*mp*ct*ct))*(dx-dxd+lambda1*(x-
xd))+(1/4*(kd2*ct*mp*l+2*kd3*A1+2*kd3*A2)/A4*(2*kd2*l+3*kd3*ct)/(2*kd1*l+3*kd2*ct)/(kd3*kd1-
kd2*kd2)*beta*(kd1-kd1f)-1/2/A4*(kd2*ct*mp*l+2*kd3*A1+2*kd3*A2)/(kd3*kd1-kd2*kd2)*beta*(kd2-
kd2f)+1/4/A4*(kd1*ct*mp*l+2*kd2*A1+2*kd2*A2)/(kd3*kd1-kd2*kd2)*beta*(kd3-kd3f)-
2*A4*(2*kd2*l+3*kd3*ct)/l/(4*A1+4*A2-3*mp*ct*ct))*(dtheta-dthetad+lambda2*(theta-thetad));